WILEY | Hindawi

Research Article

MHD Natural Convection and Sensitivity Analysis of Ethylene Glycol Cu-Al$_2$O$_3$ Hybrid Nanofluids in a Chamber with Multiple Heaters: A Numerical Study of Lattice Boltzmann Method

Meratun Junnut Anee,[1] **Md Farhad Hasan** ,[2,3] **Sadia Siddiqa** ,[4]
and Md. Mamun Molla [1,5]

[1]*Department of Mathematics & Physics, North South University, Dhaka 1229, Bangladesh*
[2]*Victoria State Government, Melbourne, Victoria 3083, Australia*
[3]*School of Computing, Engineering and Mathematical Sciences, La Trobe University, Melbourne, Victoria 3086, Australia*
[4]*School of Mechanical Engineering, University of Ulsan, Ulsan 44610, Republic of Korea*
[5]*Center for Applied and Computational Sciences (CACS), North South University, Dhaka 1229, Bangladesh*

Correspondence should be addressed to Md. Mamun Molla; mamun.molla@northsouth.edu

The present work investigates the magnetohydrodynamic (MHD) convective heat transport of hybrid nanofluids in a chamber with multiple heaters (such as hot microchips). The multiple-relaxation-time (MRT) lattice Boltzmann method (LBM) and graphics processing unit (GPU) computing are used here. The present study is important due to its relevance to real-world applications, the use of advanced simulation techniques, the consideration of hybrid nanofluids, the inclusion of magnetohydrodynamics, and the identification of critical parameters influencing heat transfer. Thermally homogeneous blocks are set at the bottom of a rectangular enclosure filled with ethylene glycol Cu-Al$_2$O$_3$ hybrid nanofluids with temperature-dependent viscosity. The cold temperature of the enclosure's left and right walls and the bottom and top surfaces is kept at adiabatic conditions. The numerical outcomes for the various parameters Rayleigh number ($10^4 \leq Ra \leq 10^6$), volume fraction ($0.00 \leq \phi \leq 0.04$), Hartmann number ($0 \leq Ha \leq 60$), and viscosity variation parameter ($0 \leq \varepsilon^* \leq 5$) are presented in terms of streamlines, isotherms, and the peripheral local and average Nusselt numbers for the heated chips. The results demonstrated that inside the chamber, the Rayleigh number (Ra), the Hartmann number (Ha), and the volume fraction of nanoparticles (ϕ) have the highest impact on the heat transfer rate for hybrid nanofluid. For increased Ha from 0 to 20, while $\phi = 0.0$ and Ra = 1 0^6, average Nusselt number decreased with 13.65%. For the same case, if the volume fraction was increased to $\phi = 0.04$, then the average Nusselt number decreased 14%. Finally, a sensitivity analysis was done to analyze the system's correctness and effectiveness to determine the significance of the specified parameters.

1. Introduction

The recent trend in electronic and mechanical engineering shows a growing interest in miniaturizing internal and external designs, components, and the final assembly of electronic units. While it provides an opportunity for progression in equipment design to meet the requirements of the associated applications, the reduction in thermal resistivity cannot be avoided due to narrowing the heat dissipation pathway. In general, heat generation could be excessively high from such delicate devices. This outcome often leads to a perceptible reduction in the efficiency and longevity of the unit as a whole. In fact, in a further complicated design, a microreactor array unit typically contains individual microreactors, and each source requires local temperature control [1]. One possible solution is to integrate insulation between each

heated source; however, it makes the process further complicated and expensive in terms of experimental investigations [2]. Therefore, an effective thermal equipment design through numerical modeling remains paramount, along with sensitivity testing, possibly with high-performance computing. There are different schematics popular among the researchers, such as considering cavities or enclosures (for example, rectangle, square, and triangular) [3–5]. This often includes the assumption of heated and cold obstacles or walls to assign the insulation and adiabatic conditions within different shaped cavities (for example, L-shaped, C-shaped, n-shaped, and wavy surface) [6–8]. In addition, a series of chips within a specified distance could be another option that thermal insulation can isolate. As a consequence, the heat transfer mechanism across each chip could be more controlled locally. These are all intended to represent the miniature device or one fraction of the internal component. Although the design methodology could be improved through the options mentioned above, considering appropriate internal components to enhance the thermal efficacy of the system should still be investigated at a microscale or mesoscale level.

Base fluids like water and oil have restricted working capacity, and there has been ongoing research for decades to look for a better option. Nanofluid is considered to be one of the most efficient alternatives to conventional base fluids due to possessing greater thermal conductivity [9–13]. The integration of nanofluids in an electronic cooling system, chip fabrication, and metal industry has been discussed recently [14–16]. While considering a single-phase nanofluid alone could improve the heat transfer application, the possible implications in any practical application will be a meticulous task to achieve. Therefore, mixing a specific volume fraction of nanoparticles with the base fluids to form a hybrid nanofluid has been considered a pragmatic solution in heat transfer devices [17]. Eastman et al. [18] reported an approximately 40% improved thermal conductivity by merely mixing 0.3% copper/volume (Cu) with ethylene glycol. The underlying concepts theoretically seem simpler to achieve, but from a manufacturer's perspective, the concerns remain. The amalgamation of such nanomaterials will make electronic equipment sophisticated. Therefore, the industries will require compelling evidence on the applicability of hybrid nanofluid before the final product in terms of stability and efficacy due to electrical current and magnetic field. The applied electrical current induces the magnetic field during the trials and testing of different equipment. A piece of prospective electronic equipment containing a hybrid nanofluid and multiple heated chips will also experience the induced magnetic field. The presence of a magnetic field typically restricts the mobility of fluid, which causes a reduction in heat transfer. A realistic observation should include the influence of magnetic field strength within the system. This is imposed by the Hartmann (Ha) number in fluid dynamics, and the concept is known as magnetohydrodynamics (MHD) [19]. In addition, due to temperature variations, the viscosity of the hybrid nanofluid should also change and hence should be considered in the system concurrently. Considering the above influential parameters, the selection of a highly accurate simulation technique should be prioritized.

Over the past three decades, researchers/engineers have paid close attention to lattice Boltzmann method (LBM) due to its exceptional capabilities in the numerical study of complicated flows, including multiphase flows, flows affected by magnetic fields, and combustion simulation [20]. LBM is one of the popular simulation techniques in nanofluid flow and heat transfer applications [21–24]. LBM has been proven to be an efficient approach through a parallel computing framework that reduces computational timescale with improved accuracy [25, 26]. LBM can be efficiently integrated with GPU computing to determine solutions at the mesoscale or microscale. The method is based on streaming and relaxation, emphasizing simulating fluid density on a specified lattice. LBM can be performed by single-relaxation-time (SRT) or multiple-relaxation-time (MRT). However, MRT-LBM has been credited to be significantly better in heat transfer applications [27]. Some recent works could be discussed in MRT-LBM that considered nanofluid in heat transfer applications.

In recent years, researchers have been interested in using magnetic fields to regulate the flow of nanofluid in managing heat transmission. The presence of a magnetic field regulates the momentum of flow and heat transfer, and studying this phenomenon on fluid flow is one of the most fascinating topics; these studies are referred to as magnetohydrodynamics (MHD) [28]. However, more information is needed to expand the work to investigate MHD and variable viscosity. Zhang and Che [29] considered MRT-LBM to study MHD natural convection of nanofluids with four square heat sources. The findings also suggested that nanofluid improved the heat transfer, but the performance was downgraded with the inclusion of the Ha number. While the results were significant and straightforward, the possible implications in heat-exchanging devices will require further sensitivity analyses and the development of correlations. Karki and Gangawane [30] considered two obstacles within their design and investigated the efficiency of hybrid nanofluid through case studies. The findings on the impact of magnetic field strength on plummeting heat transfer rate were in accord with the generic discussions above. There have been further developments in MRT-LBM-MHD studies on hybrid nanofluid to meet specific applications and associated requirements. However, there still needs to be a gap in understanding the hybrid nanofluid behavior in the presence of multiple heated sources. In addition, statistical analysis of the simulated data was barely reported in the literature.

This current study is aimed at analyzing the performance of hybrid nanofluid comparing with Al_2O_3 and Cu combining ethylene glycol base fluid and the heat transfer mechanism with six heated sources with and without magnetic field. LBM-MRT combination has been considered as the simulation technique. CUDA C parallel computing has been performed using GPU. Extensive sensitivity analyses through response surface methodology have been conducted to find an optimum solution by developing correlations among the influential parameters. The adiabatic condition has been considered between each heated block to reinforce stability and thermal insulation. This study's findings suggested that a hybrid nanofluid within a system

containing six heated chips could still be modeled for any electronic equipment. At the same time, enhanced thermal efficiency could be achieved. Furthermore, including a magnetic field provided a more realistic approach within the cavity, and the system can still be stabilized in the presence of hybrid nanofluid and thermal insulations between each heated chip. The sensitivity analyses provide elaborate explanations on thresholds and tuning the hyperparameter for industrial testing as needed.

2. Geometry of the Problem

Throughout this investigation, a rectangular cavity has been taken into consideration. This cavity has a height H and a width L, where $L = 8H$ is shown in Figure 1. This present study considers hybrid nanofluids in the cavity. The top wall and the bottom wall were considered to be adiabatic. Six heated chips were placed inside the cavity separately, and the right side and left side walls were considered cold and hence referred to as T_c. The distance between two heated chips was considered $L_2 = 0.859375H$, and the distance between the heated chips was equivalent to $L_1 = 0.726562H$. A constant magnetic field (B_0) was applied in this situation, and the influence of the magnetic effect on free convection has been thoroughly investigated. Figure 1 accurately depicts all boundary conditions applicable to the problem.

The thermophysical properties of ethylene glycol (base fluid) and Cu and Al_2O_3 nanoparticles are given in Table 1.

3. Formulation of the Problem

3.1. Dimensional Equations for Heat Transfer and Fluid Flow. In this section, continuity equation, u momentum, v momentum, and energy equations have been expressed as the following [22]:

$$\check{u}_{\check{x}} + \check{v}_{\check{y}} = 0,$$

$$\rho_{hnf}\left(\check{u}_{\check{t}} + \check{u}\check{u}_{\check{x}} + \check{v}\check{u}_{\check{y}}\right) = -\check{p}_{\check{x}} + \left(2\check{\mu}_{hnf}\check{u}_{\check{x}}\right)_{\check{x}} + \left(\check{\mu}_{hnf}\check{u}_{\check{y}}\right)_{\check{y}}$$
$$+ \left(\check{\mu}_{hnf}\check{v}_{\check{x}}\right)_{\check{y}},$$

$$\rho_{hnf}\left(\check{v}_{\check{t}} + \check{u}\check{u}_{\check{x}} + \check{v}\check{v}_{\check{y}}\right) = -\check{p}_{\check{y}} + \left(\check{\mu}_{hnf}\check{v}_{\check{x}}\right)_{\check{x}}$$
$$+ \left(2\check{\mu}_{hnf}\check{v}_{\check{y}}\right)_{\check{y}}$$
$$+ \left(\check{\mu}_{hnf}\check{u}_{\check{y}}\right)_{\check{x}}$$
$$+ g(\rho\beta)_{hnf}\left(\check{T} - T_c\right)$$
$$- \sigma_{hnf}B_o^2\check{v},$$

$$\check{T}_{\check{t}} + \check{u}\check{T}_{\check{x}} + \check{v}\check{T}_{\check{y}} = \alpha_{hnf}\left(\check{T}_{\check{x}^2} + \check{T}_{\check{y}^2}\right),$$
$$(1)$$

where ρ_{hnf} is the effective density and $(\rho\beta)_{hnf}$ is the thermal expansion coefficient of the nanofluid. Here, σ_{hnf} is

the electrical conductivity of the nanofluid, respectively. In the following equations, the effective density ρ_{hnf} and thermal expansion coefficient β_{hnf} are defined with these symbols [32, 33]. $(\rho C_p)_{nf}$ is the heat capacitance. Here, ρ_{hnf} stands for effective density (hybrid nanofluid).

$$\rho_{nf} = \rho_f(1 - \phi) + \rho_s\phi,$$

$$\rho_{hnf} = \rho_f(1 - \phi) + \phi_{Al_2O_3}\rho_{Al_2O_3} + \phi_{Cu}\rho_{Cu}, \quad (2)$$

$$\left(\rho C_p\right)_{nf} = \left(\rho C_p\right)_f(1 - \phi) + \left(\rho C_p\right)_s\phi.$$

Through the following two equations, the heat capacitance coefficient of a hybrid nanofluid is determined [32, 33]:

$$\left(\rho C_p\right)_{hnf} = \left(\rho C_p\right)(1 - \phi)_f + \left(\rho C_p\right)\phi,$$

$$\left(\rho C_p\right)_{hnf} = \left(\rho C_p\right)_f(1 - \phi) + \phi_{Al_2O_3}\left(\rho C_p\right)_{Al_2O_3} + \phi_{Cu}\left(\rho C_p\right)_{Cu}.$$
$$(3)$$

ϕ denotes the volume fraction for a hybrid nanofluid.

$$\phi = \phi_{Al_2O_3} + \phi_{Cu},$$

$$\beta_{hnf} = \beta_f(1 - \phi) + \beta_s\phi.$$
$$(4)$$

Electrical conductivity is expressed as follows [32, 33]:

$$\sigma_{hnf} = \sigma_{bf}\left[1 + \frac{3\left(\left(\sigma_{s_{bf}}/\sigma_f\right) - 1\right)\phi}{\left(\left(\sigma_{s_{bf}}/\sigma_{bf}\right) + 2\right) - \left(\left(\sigma_{s_{bf}}/\sigma_{bf}\right) - 1\right)\phi}\right],$$

$$\sigma_{bf} = \sigma_f\left[1 + \frac{3\left(\left(\sigma_{s_f}/\sigma_f\right) - 1\right)\phi}{\left(\left(\sigma_{s_f}/\sigma_f\right) + 2\right) - \left(\left(\sigma_{s_f}/\sigma_f\right) - 1\right)\phi}\right].$$
$$(5)$$

Here, α_{nf} is the thermal diffusivity denoted by the following equation [32, 33]:

$$\alpha_{hnf} = \frac{k_{hnf}}{\left(\rho C_p\right)_{hnf}}, \quad (6)$$

where μ_f is the viscosity of the base fluid.

The effective temperature-dependent thermal conductivity k_{hnf} of hybrid nanofluid is calculated based on the experimental data, reflected through the correlation [34] as

$$k_{hnf} = k_{bf}\frac{k_s + 2k_{bf} - 2\phi\left(k_{bf} - k_s\right)}{k_s + 2k_{bf} + \phi\left(k_{bf} - k_s\right)},$$

$$k_{bf} = k_f\frac{k_s + 2k_f - 2\phi\left(k_f - k_s\right)}{k_s + 2k_f + \phi\left(k_f - k_s\right)}.$$
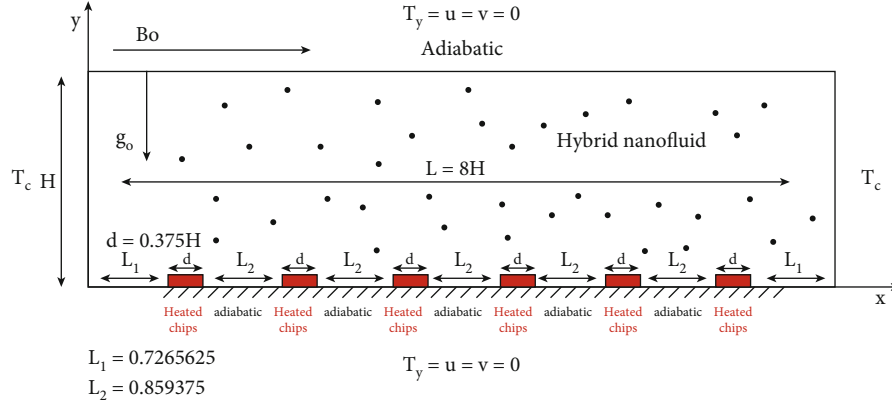$$(7)$$

Figure 1: Physical model of the six heaters in a rectangular cavity and boundary conditions.

Table 1: Thermophysical properties of base fluid ethylene glycol and Cu and Al_2O_3 nanoparticles [31].

Properties	Ethylene glycol	Cu (copper)	Al_2O_3 (alumina)
ρ (kg m^{-3})	1115	8933	3970
c_p (J kg^{-1} K^{-1})	2430	385	765
k (W m^{-1} k^{-1})	0.253	401	40
β (k^{-1})	57×10^{-5}	1.67×10^{-5}	0.85×10^{-5}
σ (S/m)	1.07×10^{-4}	59.6×10^6	35×10^6
μ (Nm^{-2}s)	1.73×10^{-3}		

The Brinkman model [35, 36] combined with the temperature-dependent viscosity model of Ling and Dibbs [37] defines the hybrid nanofluid's effective dynamic viscosity. The hybrid nanofluid's ($\breve{\mu}_{nf}$) viscosity may be demonstrated by the following [32, 33]:

$$\mu_{hnf} = \frac{\mu_f}{(1-\phi)^{2.5}[1+\varepsilon(T-T_c)]}. \tag{8}$$

3.2. Nondimensional Governing Equations.
The following are expressions of the dimensionless equations for continuity, u momentum, v momentum, and energy [33]:

$$u_x + v_y = 0,$$

$$u_t + uu_x + vu_y = -\frac{\rho_f}{\rho_{hnf}} p_x + \frac{1}{(1-\phi)^{2.5}} \frac{\Pr\left(\sqrt{\text{Ra}}\right)^{-1}}{(1-\phi) + \left(\phi\rho_s/\rho_f\right)}$$

$$\cdot \left[\left(2\frac{\mu_{hnf}}{\mu_f} u_x \right)_x + \left(\frac{\mu_{hnf}}{\mu_f} u_y + \frac{\mu_{hnf}}{\mu_f} v_x \right)_y \right],$$

$$v_t + uv_x + vv_y = -\frac{\rho_f}{\rho_{hnf}} p_y + \frac{1}{(1-\phi)^{2.5}} \frac{\Pr\left(\sqrt{\text{Ra}}\right)^{-1}}{(1-\phi) + \left(\phi\rho_s/\rho_f\right)}$$

$$\cdot \left[\left(2\frac{\mu_{hnf}}{\mu_f} v_y \right)_y + \left(\frac{\mu_{hnf}}{\mu_f} u_y + \frac{\mu_{hnf}}{\mu_f} v_x \right)_x \right]$$

$$+ \frac{\rho_f \Pr \beta_{hnf}}{\rho_{hnf} \beta_f} \theta - \frac{\sigma_{hnf}}{\sigma_f} \frac{\rho_f}{\rho_{hnf}} \frac{\Pr \text{Ha}^2}{\sqrt{\text{Ra}}} v,$$

$$\theta_t + u\theta_x + v\theta_y = \frac{\alpha_{hnf}}{\alpha_f} \frac{1}{\sqrt{\text{Ra}}} \left(\theta_{xx} + \theta_{yy} \right). \tag{9}$$

The nondimensionalized effective dynamic viscosity μ_{hnf} becomes

$$\frac{\breve{\mu}_{hnf}}{\mu_f} = \frac{1}{(1-\phi)^{2.5}(1+\varepsilon^*\theta)}. \tag{10}$$

Here, ε^* denotes the viscosity variation parameter.

$$\varepsilon^* = \varepsilon\Delta T. \tag{11}$$

The following list contains the dimensionless variables that were utilized to create the nondimensional equations [33]:

$$x = \frac{\breve{x}}{H},$$

$$y = \frac{\breve{y}}{H},$$

$$u = \frac{\breve{u}}{(\alpha_f/H)\sqrt{\text{Ra}}},$$

$$v = \frac{\breve{v}}{(\alpha_f/H)\sqrt{\text{Ra}}},$$

$$p = \frac{\breve{p}}{\rho_f(\alpha_f/H)^2\text{Ra}},$$

$$t = \frac{\check{t}\sqrt{\text{Ra}}}{\left(H^2/\alpha_f\right)},$$

$$\theta = \frac{T - T_C}{\Delta T},$$

$$\Delta T = T_w - T_c,$$

$$\text{Ha} = \sqrt{\frac{\sigma_f}{\mu_f}}HB_0,$$

$$\text{Ra} = \frac{g\beta_f\Delta TH^3}{\alpha_f\nu_f}. \tag{12}$$

3.3. Average Rate of Heat Transfer Calculation. Equation (13) for MHD convection has been used to calculate heat transport for one chip only by average Nusselt values. In the present problem, six heated chips were considered. Equation (13) will change according to the number of chips used in the system. As each chip has 3 sides, it was needed to calculate the average Nusselt numbers ($\bar{\text{Nu}}$) for sides as follows:

For the chip 1 case, the following could be expressed [38]:

$$\bar{\text{Nu}}_1 = \frac{1}{3}\left(\frac{1}{y_2 - y_1}\int_{y_1}^{y_2} -\frac{\partial T}{\partial x}\bigg|_{x=x_1} dy + \frac{1}{y_2 - y_1}\int_{y_1}^{y_2}\right.$$
$$\left. -\frac{\partial T}{\partial x}\bigg|_{x=x_2} dy + \frac{1}{x_2 - x_1}\int_{x_1}^{x_2} -\frac{\partial T}{\partial y}\bigg|_{y=y_2} dx\right). \tag{13}$$

Therefore, the average Nusselt number $\bar{\text{Nu}}$ for the six chips could be determined as the following [38]:

$$\bar{\text{Nu}} = \frac{1}{6}\left(\bar{\text{Nu}}_1 + \bar{\text{Nu}}_2 + \bar{\text{Nu}}_3 + \bar{\text{Nu}}_4 + \bar{\text{Nu}}_5 + \bar{\text{Nu}}_6\right). \tag{14}$$

4. Multiple-Relaxation-Time Lattice Boltzmann Method (MRT-LBM)

The D2Q5 and D2Q9 MRT-LBM theories have been employed in calculating physical variables for the current investigation, including fluid velocity, temperature, and solute concentration [38–41]. Below is a quick discussion of how the equations were developed.

$$\mathbf{f}(\mathbf{r} + \mathbf{e}_i\Delta t, t + \Delta t) - \mathbf{f}(\mathbf{r}, t) = -\mathbf{M}^{-1}\mathbf{S}[m(\mathbf{r}, t) - \mathbf{m}^{eq}(\mathbf{r}, t)]$$
$$+ \mathbf{M}^{-1}\left(\mathbf{I} - \frac{\mathbf{S}}{2}\right)\mathbf{F}(\mathbf{r}, t), \tag{15}$$

$$\mathbf{g}(\mathbf{r} + \mathbf{e}_i\Delta t, t + \Delta t) - \mathbf{g}(\mathbf{r}, t) = -\mathbf{N}^{-1}\mathbf{S_T}\left[\mathbf{m_T}(\mathbf{r}, t) - \mathbf{m}_T^{eq}(\mathbf{r}, t)\right], \tag{16}$$

where $\mathbf{r} = (\bar{x}, \bar{y})$ and $\mathbf{f} = (f_0, f_1, f_2, \cdots\cdots, f_8)^T$. In this instance, the vector moments are $\mathbf{m} = (m_0, m_1, m_2, \cdots\cdots, m_8)^T$ and $\mathbf{m}^{eq} = (m_0{}^{eq}, m_1{}^{eq}, m_2{}^{eq}, \cdots\cdots, m_8{}^{eq})^T$, and the driving forces include $\mathbf{F} = (F_0, F_1, F_2, \cdots\cdots, F_8)^T$. In the same way, for D2Q5 model, $g = (g_0, g_1, g_2, \cdots\cdots, g_4)^T$ are the density-distributed functions for the thermal field. The forcing scheme used in Eq. (15) to impose the external force can significantly impact result accuracy [42].

The velocity and moment spaces are transformed using a linear transformation for the momentum equation, considering $\mathbf{m} = \mathbf{Mf}$ which means that $\mathbf{f} = \mathbf{M}^{-1}\mathbf{m}$, where

$$\mathbf{M} = \begin{bmatrix} 1 & 1 & 1 & 1 & 1 & 1 & 1 & 1 & 1 \\ -4 & -1 & -1 & -1 & -1 & 2 & 2 & 2 & 2 \\ 4 & -2 & -2 & -2 & -2 & 1 & 1 & 1 & 1 \\ 0 & 1 & 0 & -1 & 0 & 1 & -1 & -1 & 1 \\ 0 & -2 & 0 & 2 & 0 & 1 & -1 & -1 & 1 \\ 0 & 0 & 1 & 0 & -1 & 1 & 1 & -1 & -1 \\ 0 & 0 & -2 & 0 & 2 & 1 & 1 & -1 & -1 \\ 0 & 1 & -1 & 1 & -1 & 0 & 0 & 0 & 0 \\ 0 & 0 & 0 & 0 & 0 & 1 & -1 & 1 & -1 \end{bmatrix}. \tag{17}$$

Within equation (15) implies that S represents a diagonal collision matrix at the moment space having nine eigenvalues ranging from 0 to 2, presented in

$$\mathbf{S} = \mathbf{diag}\ [s_0, s_1, s_2, s_3, s_4, s_5, s_6, s_7, s_8], \tag{18}$$

where $s_0 = s_3 = s_5 = 1.0$, $s_1 = s_2 = 1.4$, $s_4 = s_6 = 1.2$, and $s_7 = s_8 = 1/\tau$. In this case, $\tau = 3\nu_{hnf} + 12$ is the relaxation time, and ν_{hnf} is the kinematic viscosity specified by the following relation [38]:

$$\nu_{hnf} = \frac{1}{(1 - \phi)^{2.5}}\frac{\text{Pr}\left(\sqrt{\text{Ra}}\right)^{-1}}{(1 - \phi) + \left(\phi\rho_s/\rho_f\right)}\frac{\mu_{hnf}}{\mu_f}. \tag{19}$$

The D2Q9 model's density distribution function e_i is specified as in [41] in the direction of velocity.

In Equation (15), $\mathbf{m^{eq}}$ is expressed by [38]

$$\mathbf{m}^{eq} = \left[\rho, 2\rho + 3|j|, \rho - 3|j|, j_x, -j_x, j_y, -j_y, \left(j_x^2 - j_y^2\right), j_xj_y\right], \tag{20}$$

where $(j_x, j_y) = (\rho\bar{u}, \rho\bar{v})$ and $|j| = j_x^2 + j_y^2$. Here, [43] provides the values for ρ and $\mathbf{u}$:

$$\rho = \sum_{i=0}^{8} f_i,$$
$$\mathbf{u} = \frac{1}{\rho}\sum_{i=0}^{8} f_i e_i. \tag{21}$$

The collision matrix $\mathbf{N}$ for D2Q5 is provided below:

$$\mathbf{N} = \begin{bmatrix} 1 & 1 & 1 & 1 & 1 \\ 0 & 1 & 0 & -1 & 0 \\ 0 & 0 & 1 & 0 & -1 \\ -4 & 1 & 1 & 1 & 1 \\ 0 & 1 & -1 & 1 & -1 \end{bmatrix}. \tag{22}$$

The five eigenvalues of S_T for the D2Q5 model are expressed as follows [38]:

$$S_T = \text{diag}\,[s_0, s_\alpha, s_\alpha, s_e, s_v]. \tag{23}$$

As indicated in eqs. (24) and (25), the explanation and formulation of s_i values have been provided in detail in [38, 43]:

$$s_0 = 1, \frac{1}{s_e} - \frac{1}{2} = \frac{1}{s_v} - \frac{1}{2} = \frac{1}{6}. \tag{24}$$

In this case, s_α is determined as explained in Mezrhad et al. [44]:

$$s_\alpha = \frac{1}{(1/2) + 5\alpha}. \tag{25}$$

The thermal diffusivity α is determined as follows [38, 43]:

$$\alpha = \frac{\alpha_{hnf}}{\alpha_f} \frac{1}{\sqrt{Ra}}. \tag{26}$$

The effective thermophysical properties of the nanoparticles that have been used in this simulation through equations (19) and (26) are shown in Table 2.

Equilibrium moments [38, 43] $\mathbf{m}_T^{eq}$ for the distribution function g_i are

$$\mathbf{m}_T^{eq} = [T, \bar{u}T, \bar{v}T, aT, 0]. \tag{27}$$

The temperature of the fluid [38, 43], T, are calculated as

$$T = \sum_{i=0}^{4} g_i. \tag{28}$$

4.1. The Boundary Conditions.

The boundary conditions used in this fluid simulation problem specify that the walls in the simulation are modeled using the bounceback condition. This means that fluid particles that collide with the wall are bounced back in the opposite direction, preserving the overall density of the fluid. Additionally, the walls between the chips are specified as thermally adiabatic, meaning that they do not exchange heat with the fluid. For these walls, the zero gradient condition is used, which means that the temperature gradient at the wall is set to zero.

TABLE 2: The effective thermophysical properties of the nanoparticles that have been used in this simulation (here, the viscosity is calculated for $\varepsilon^* = 0$).

ϕ	ρ_{hnf}/ρ_f	μ_{hnf}/μ_f	k_{hnf}/k_f	α_{hnf}/α_f
0.0	1.0	1.0	1.0	1.0
0.01	1.047955	1.025444	1.030198	1.028210
0.02	1.095910	1.051804	1.061009	1.056923
0.03	1.143865	1.079122	1.092454	1.086155
0.04	1.191821	1.107444	1.124552	1.115923

Figure 2 demonstrates the no-slip condition for the current model.

The known temperature of the walls denoted as T_{wall} is specified and used in the simulation. This temperature is used to calculate the heat exchange between the fluid and the wall or to set the wall's temperature in case of the zero gradient condition. The known temperature T_{wall} is used as follows [44]:

$$g_i(\mathbf{r}, b) = 2T_{\text{wall}} \frac{(1 + (a/4))}{5} - g_i^c(c_0). \tag{29}$$

Here, $a = -2$ for D2Q5 model [44].

For an adiabatic wall, the antibounceback conditions are shown [44]:

$$g_i(r, b) = g_i^c(x, t). \tag{30}$$

The geometry for the present problem from Figure 1 follows two different methods for adiabatic and cold walls. The temperature condition for the cold and adiabatic walls has been given below:

(i) The right wall has a cold temperature, and the condition is $g_3 = -g_1$

(ii) The left wall has a cold temperature, and the condition is $g_1 = -g_3$

(iii) The adiabatic condition is present on the bottom wall $g_{i,0} = g_{i,1}$

(iv) The adiabatic situation at the top wall is $g_{i,N} = g_{i,N-1}$

The macroscopic quantities are calculated as follows [44]:

$$\rho = \sum_{i=0}^{8} h_i,$$

$$\bar{\mathbf{u}} = \frac{1}{\rho} \sum_{i=0}^{8} h_i \mathbf{e}_i, \tag{31}$$
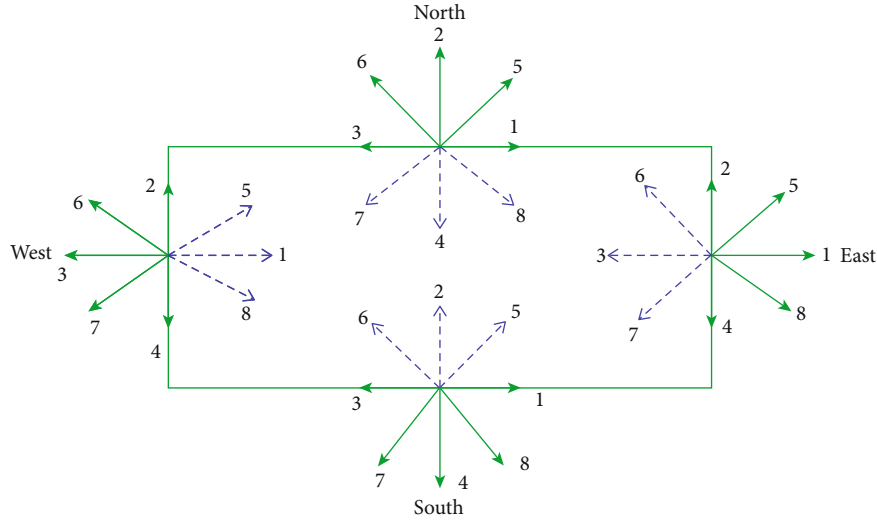
$$T = \sum_{i=0}^{4} g_i.$$

FIGURE 2: Two-dimensional structure for bounceback condition applied to the walls.

TABLE 3: Grid independence test for the different Ra and Hartmann number Ha while $\varepsilon^* = 5$, Pr = 16.6, and $\phi = 0.04$ in terms of the average Nusselt number (Nu).

Lattice size	Ha = 0	Ha = 20	Ha = 60
Ra = 10^5			
Grid 1: 512 × 64	4.3423 (0.98%)	3.5212 (1.87%)	1.8921 (3.37%)
Grid 2: 1024 × 128	4.3001 (0.00%)	3.4566 (0.00%)	1.8305 (0.00%)
Grid 3: 2048 × 256	4.2217 (1.82%)	3.4123 (1.28%)	1.8017 (1.57%)
Ra = 10^6			
Grid 1: 512 × 64	9.0412 (8.49%)	6.9632 (7.96%)	4.7051 (2.31%)
Grid 2: 1024 × 128	8.3333 (0.00%)	6.4496 (0.00%)	4.5987 (0.00%)
Grid 3: 2048 × 256	8.1292 (2.45%)	6.3741 (1.17%)	4.5132 (1.86%)

5. Model Validations

The grid independence test is a useful tool for evaluating the accuracy of a numerical model. The simulation should reach a consistent solution by fine-tuning the grid or mesh. The solution is not numerically stable or reliable if the results drastically vary with changing grid resolutions. Tests for grid independence assist in identifying the simulation's convergence behavior. As the grid resolution is raised, convergence describes the propensity of the solution to become closer to a steady state. It is easy to determine whether the solution is convergent or requires more refining by comparing the results obtained with various grid sizes. The variation in results from different grid sizes gives a clue as to the mistake brought about by grid discretization.

5.1. Grid Independence Test. To verify the validity and accuracy of numerical simulations, grid independence tests were performed. These tests assisted in validating numerical correctness, evaluating convergence behavior, estimating errors, and optimizing computational resources by comparing results obtained from different grid resolutions. In Table 3, three lattice arrangements have been selected for the six

heaters: for case 1: 512 × 64, case 2: 1024 × 128, and case 3: 2048 × 256 along the $x × y$ directions, respectively. For refining the grid sizes, the errors are decreasing. So, it is evident from a visual assessment that case 2 (1024 × 128) is enough for the current investigation.

The grid independence test also provided for velocity and temperature distribution is depicted in Figures 3(a) and 3(b), respectively, for the two different Rayleigh numbers (Ra = 10^5 and 10^6) while Pr = 16.6, $\varepsilon^* = 5$, $\phi = 0.04$, and Ha = 40 at $y = 0.5$. These figures show evidence that the results are very close for the higher two grid arrangements.

5.2. Code Validation for a Single Heater. The code validation was performed by comparing the results with the experimental investigation by Nardini et al. [45] for a single heater placed at the bottom wall in a square cavity. The left and right vertical walls of the cavity were fixed at a cold temperature of 291.16 K, and the heater was at 310.65 K. Other than the heater, the bottom wall was thermally adiabatic. At the top and bottom walls, a Plexiglas was used with a constant heat convection coefficient of $8\,Wm^2K^1$. The qualitative comparison is shown in Figure 4 regarding the isotherms.
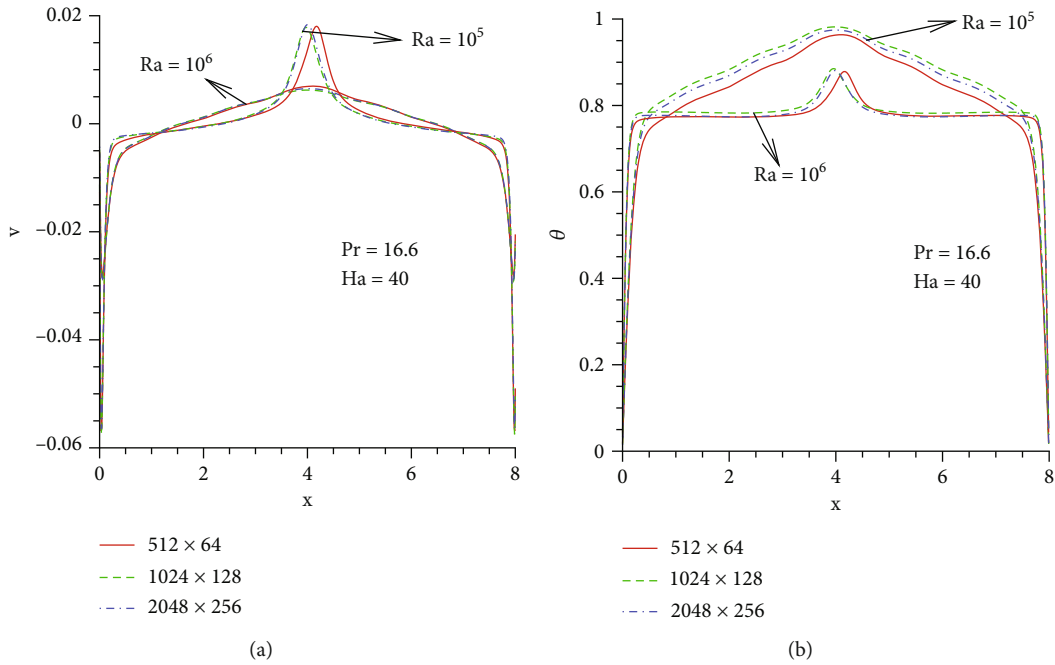
(a)

(b)

FIGURE 3: Grid independent test for the different Rayleigh numbers in terms of the (a) vertical velocity v and (b) temperature θ while Pr = 16.6, $\varepsilon^* = 5$, $\phi = 0.04$, and Ha = 40 at $y = 0.5$.
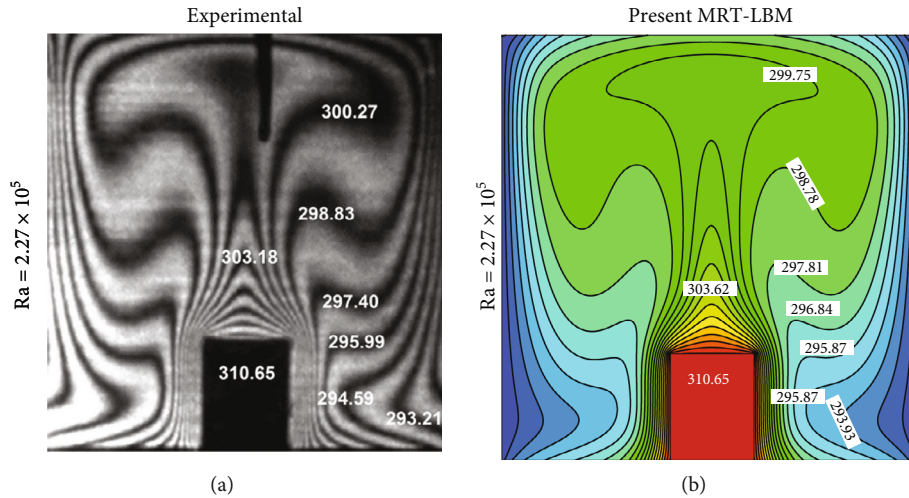

(a)

(b)

FIGURE 4: Code validation for a single heater in terms of isotherms with the (a) experimental results of Nardini et al. [45] and (b) present MRT-LBM results while Ra = 2.27×10^5, $\varepsilon^* = 0$, Ha = 0, $\phi = 0.0$, and Pr = 0.71.

The agreement was found to be in accord with the published work of Nardini et al. [45].

5.3. Code Validation for the Magnetic Field Effect.

The existing MRT-LBM code is quantitatively validated for the magnetic field effects in a side heated square cavity. Table 4 shows the comparison by $\overline{\mathrm{Nu}}$. The results exhibit excellent agreement quantitative with the findings of Rudraiah et al. [46] by the finite difference method (FDM) for the Navier-Stokes equation. From this comparison, it was ensured that the numerical accuracy was satisfactory by the present MRT-LBM.

5.4. Code Validation for the Nanofluid.

In Figure 5, another quantitative comparison of the present average Nusselt numbers with the experimental average Nusselt numbers of Ho et al. [47] for Al_2O_3-water nanofluid in a side heated square enclosure has been done for the different Rayleigh numbers while $\phi = 0.03$ and Pr = 7.002. This quantitative comparison also leads to the validity of the present MRT-LBM code for the nanofluid flow simulation. The results show that the error is 0% at Ra = 10^6 and, in other places, errors are as low as 0.1%, 1.04%, and 0.38%, respectively. That means the numerical accuracy was satisfactory by the present MRT-LBM.

TABLE 4: Comparison for magnetic field effects on the average Nusselt number ($\overline{Nu}$) is shown with the results of Rudraiah et al. [46] where Pr = 0.733, $\varepsilon^* = 0$, Ha = 0, and $\phi = 0.0$. NSE stands for the Navier-Stokes equation.

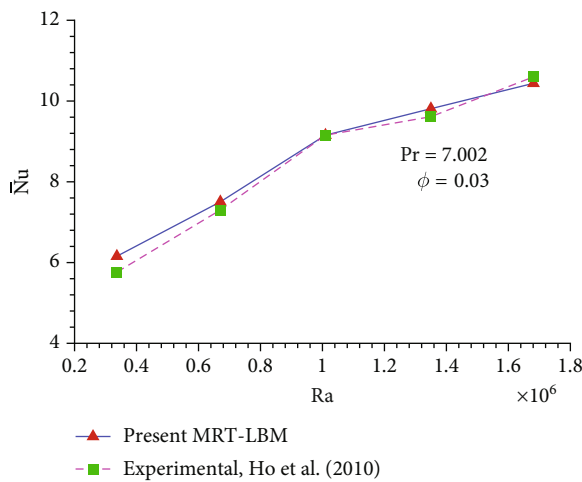| Ra = GrPr	Ha	Present MRT-LBM	NSE-FDM [46]	% $|\Delta|$
	0	2.5444	2.5188	1.006
	10	2.2426	2.2234	0.856
1.466×10^4	50	1.0743	1.0856	1.051
	100	1.0122	1.0110	0.119
	0	5.0121	4.9198	1.842
	10	4.8636	4.8053	1.198
1.466×10^5	50	2.8384	2.8442	0.204
	100	1.4613	1.4317	2.026

FIGURE 5: Present average Nusselt numbers are compared with the experimental average Nusselt numbers of Ho et al. [47] for Al_2O_3-water nanofluid while $\varepsilon^* = 0$, $\phi = 0.03$, Pr = 7.002, and Ha = 0.

6. Results and Discussions

The study of magnetohydrodynamic (MHD) natural convection of hybrid nanofluids in a chamber with six heaters holds paramount significance in the realm of thermal and fluid dynamics research. This sophisticated simulation technique allows for a detailed and accurate investigation of the complex interplay between magnetic fields, natural convection, and the hybrid nanofluids' intricate heat transfer characteristics. By employing MRT-lattice Boltzmann methods, researchers gain a powerful tool to analyze and optimize the thermal performance of nanofluids in practical applications. The inclusion of MHD effects adds a layer of complexity, enabling the exploration of magnetically influenced convective heat transfer. This simulation serves as a valuable resource in the development of efficient cooling systems and heat exchangers. For the different applications, it is necessary to understand and select the accurate value of the parameters to make an efficient design. In the present study, we set up different values of the parameters and observed the variation of results due to the effect of change in the parameter values. The parameters considered for this

work are thermal Rayleigh number (Ra) from 10^4 to 10^6, volume fraction (ϕ) = 0.00 to 0.04, Hartmann number (Ha) = 0 to 80, viscosity variation parameter $\varepsilon^* = 0$ to 5, and Prandtl number Pr = 16.6. The simulation assumptions of this work are as follows:

(i) The study is on laminar incompressible natural convection flow

(ii) The fluid is Newtonian

(iii) The thermal conductibility of the fluid is constant

(iv) The present investigation is for the two-dimensional domain

(v) The investigation is for the single-phase hybrid nanofluid

6.1. Effects of Thermal Rayleigh Numbers. The ratio of buoyant to viscous forces in a fluid system is described by the dimensionless thermal Ra number. Convection, mixing, and heat transfer are just a few of the fluid dynamic processes that can be significantly impacted by this parameter. The fluid is generally stable at low thermal Ra numbers, and heat is mostly transported by conduction. Convection takes over as the dominant mode of heat transmission when the thermal Ra number increases. The heat transmission rate may become saturated as a result of this. Thermal Ra number has complicated impacts on fluid systems that rely on the particulars of the system, such as the fluid characteristics, the boundaries, and the imposed circumstances.

Figures 6(a)–6(c) depict streamlines and isotherms for variations in the Rayleigh number Ra = 10^4, 10^5, and 10^6, and other parameters were set at $\varepsilon^* = 2$, $\phi = 0.04$, and Ha = 40. Six distinct heated blocks have been taken into consideration in the current investigation. Overall, the streamlines demonstrated symmetrical patterns in this instance. The same trend can be seen in isotherms as well. At low Ra numbers, flow rates are dominated by conduction. Two mirrored vortices with opposite rotational characteristics were developed for each Ra number, one for each enclosure. These two vortices were found to be stretching themselves as the Ra numbers increased. The consistency of the vortex was apparent. According to the stream function, blue and red were denoted as negative and positive, respectively. The stream function with the opposite direction also allowed the observation of the magnitudes of the velocity. As Ra grows, the magnitude of the stream function grows as well. The center magnitude grows from 1.91 to 26.63 when Ra grows from 10^4 to 10^6. In the y direction, isolines were observed to be parallel, indicating the conduction's dominance. Isotherms nearly appeared to be parallel to the top and bottom walls, as shown in Figures 6(d)–6(f). Between the cold walls and the heated chips, a greater temperature gradient was noticed. Isotherms were seen to be distorted in the opposite direction from the central area (to the cold walls). The heated chips were positioned in the cavity's middle, primarily aiding in the distortion of the isotherm. Isolines in the central section have a lower temperature
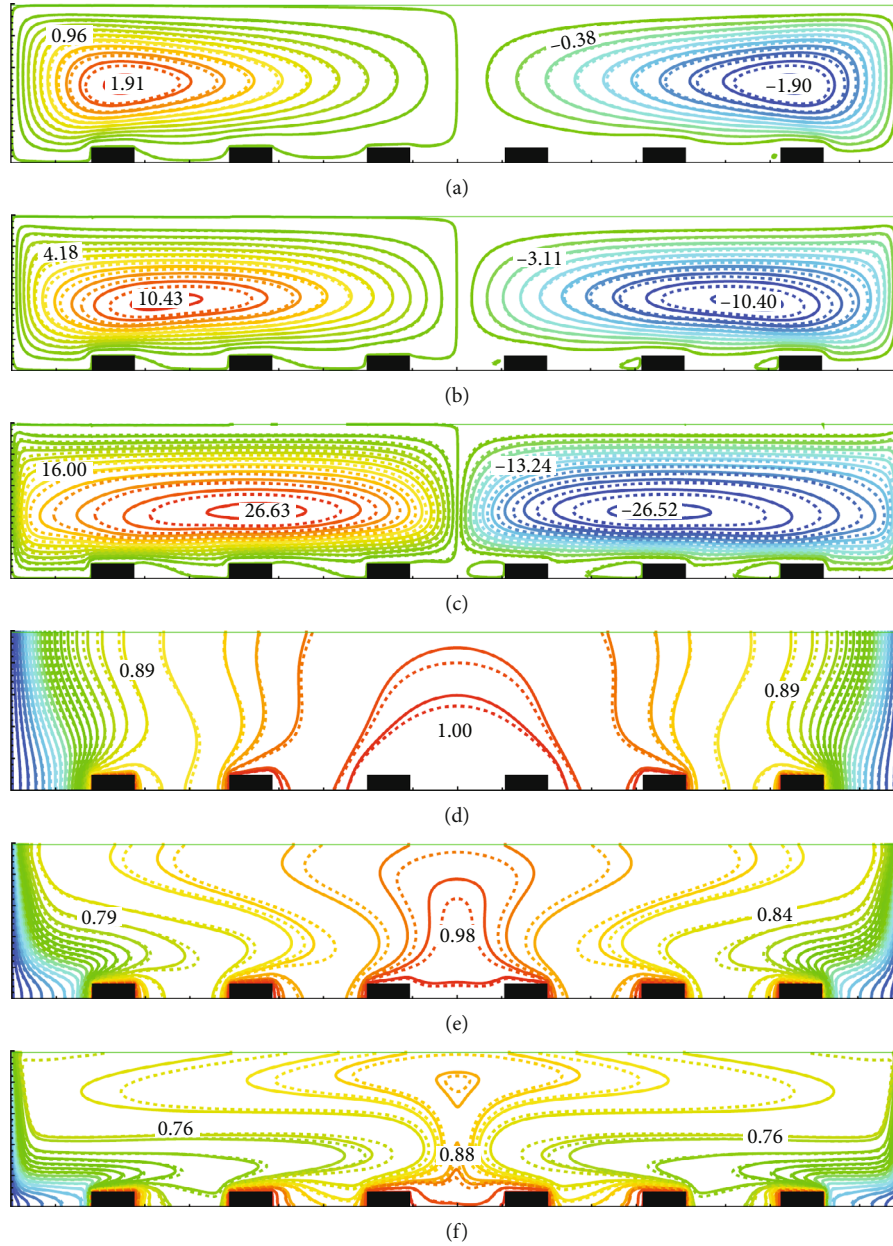
FIGURE 6: Streamlines and isotherms for (a, d) Ra = 10^4, (b, e) Ra = 10^5, and (c, f) Ra = 10^6 while $\varepsilon^* = 2$ and Ha = 40 are fixed and here solid lines for $\phi = 0.04$ and dashed lines for $\phi = 0.00$.

gradient and appear to be spread out toward the cold walls. When the Ra number was comparatively lower, fluid mobility got delayed near the center and progressively experienced augmented mobility as it approached the cold walls. Due to increased velocity gradients, it was also seen that the isotherms were denser toward the edges of the cold walls. By managing the hybrid nanofluid flow, all isothermal lines were properly structured, regular, and compressed for the MHD effect.

As Ra was increased, the core vortex gradually shifted from being close to the cold walls to being in the middle of the heated chips, and this was especially true when Ra was increased to a value of Ra = 10^6 (Figure 6(f)). Due to the

top wall's adiabatic state, the adjacent temperature increased due to increasing the Ra number. However, the temperature was consistently lower in the proximity of the left and right walls (cold). It is significant that when Ra grows, fluid velocity inside the cavity also increases. At first, the hot fluid initially rises to the top of the cavity, aiding in accelerating the flow. Eventually, the vortex was surrounded by this hot fluid inside the cavity. The buoyancy force is another physical principle behind the acceleration of fluid flow. Buoyancy force increases along with an increase in Ra value. This force mostly improves fluid flow. It is important to note that the magnetohydrodynamic effect was also in charge of the isotherm and streamline distortion but was unable to alter the

lower middle region. Due to the magnetic field effect in this cavity, the Lorentz force was generated, slightly reducing the convective heat transfer flow rate. Including ϕ within the system (solid lines) also showed marginal improvement in both streamlines and isotherms. Despite assigning Ha = 40 within the system, the inclusion of nanoparticles still showed better stability than the base fluid ($\phi = 0.00$).

From the observations mentioned above, the patterns in the streamlines changed slightly with increasing viscosity. It caused decrements in fluid flow and lessened the strength of the vortex point so that it turned two vortices into one. So if it is required to expand the region of the flow phenomena within the cavity, it will be prudent to choose the smallest viscosity. This can control the flow phenomena of a fluid-changing viscosity parameter.

6.2. Impacts of Hartmann Number. To explain the impact of magnetic field strength on a flow system, a Ha number is assigned. The magnetic field impact on fluid flow is minimal for low Ha numbers. The influence of the magnetic field on the fluid strengthens as the Ha number increases, and flow patterns will become more intricate and stable due to restricted mobility. The interaction of the magnetic field with the fluid flow can lead to more significant mixing and heat transfer. The Ha number can affect the behavior of the suspended nanoparticles in a hybrid nanofluid. The nanoparticles' transport and thermal characteristics may alter due to their alignment or aggregation in the magnetic field. These phenomena may impact the hybrid nanofluid system's total heat transfer performance inside an electronic equipment or microchip.

The influence of the magnetic field on the streamlines and isotherms of hybrid nanofluid is depicted in Figure 7. Other parameters had constant values such as Ra = 10^5, ε^* = 3, and $\phi = 0.04$. Figure 7 shows the flow field evolution of the hybrid nanofluid inside the cavity. A rising Ha number shows that the magnetic field was getting stronger proportionately, which weakened the flow field. Data shows that when Ha grows from 0 to 80, the magnitude of the stream function drops from 21.6 to 4.36. It also involves the Lorentz force. This Lorentz force imposed restrictions on the mobility of the fluid particles. Consequently, this characteristic impeded heat convection, resulting in a relative increase in the conduction process.

Ha = 0 indicated the absence of a magnetic field within the cavity. Therefore, in this instance, fluid flow did not get disrupted. It could be seen from Figures 7(a)–7(c) that two vortices were developed at the interface between the cold and multiple heaters layer. The density of the streamlines was reduced as Ha increased from 0 to 80, indicating the negative effect of the Ha flow function. The flow direction of each vortex pair remained opposite, as mentioned in the previous explanation of the effects of Ra number variation. It showed that while the flow rate got restricted due to the magnetic field, it did not change the rotational pattern of the streamlines. Since there was no magnetic field influence on Figure 7(a) and Ra = 10^5 was taken into account throughout this part of the investigation, convection was inferred to be the dominant mode of heat transmission for fluids since

larger Ra numbers usually reinforce convective heat transfer. Most of the heat produced by the several heated blocks was directed toward the cavity's cold walls.

For the magnetohydrodynamic effect, the considered hybrid nanofluid for the current study was electrically conducting fluid in the presence of the magnetic field. The diffusive magnetic layer, also known as a Hartmann layer, is created when the Hartmann number is increased to Ha = 20. These layers have various electric characteristics [48–50]. The magnetic field created a force that opposed the flow direction. According to Figures 7(e)–7(h), isothermal lines were heavily impacted inside the cavity as Ha increased concurrently, which caused a reduction in the heat transfer rate. Fluid convection and velocity once more diminished due to the Lorentz force and an increased Ha number. Additionally, it may be claimed that the heat transmission method switched from convection to conduction as the Ha number increased. It could be observed that Ha = 80 had the greatest impact on fluid velocity and temperature profile in Figure 7(d). As per Figures 7(e)–7(h), the findings suggested the control mechanism of heat transfer and associated development across each heated chip. If it remains necessary to locally increase the temperature across chips 2-4, increasing the Ha number provides an immediate solution. This should also be implemented in the presence of ϕ as it adds more stability to the system, which will likely increase the durability of the internal components of electronic equipment.

6.3. Influence of Temperature-Dependent Viscosity. The temperature-dependent viscosity can significantly affect streamlines and isotherms in MHD convection. According to Figure 8, the viscosity's variation with temperature impacted the overall convection patterns, producing complicated and intriguing effects. However, the changes were more visible in terms of isotherms, as seen in Figures 8(e)–8(h). The heat transmission rate was slowed down by increased viscosity. In contrast, a reduced viscosity would result in more fluid flow, improving heat transmission. The strength of the magnetic field also affected the magnetic field's ability to promote or inhibit the MHD convective patterns. In this case, Ha = 60 was imposed.

The impact on streamlines (Figures 8(a)–8(d) indicated similar patterns as earlier discussion, including a pair of vortices with opposite rotational characteristics. Since Ha and Ra numbers were consistent, the flow patterns had no immediate impact. However, temperature-dependent viscosity exhibited a noticeable impact on isotherms as it is related to temperature gradients, as shown in Figures 8(e)–8(h). As ε^* increased, the isothermal distribution gradually narrowed down. A more influential impact could be observed at the center (between chip 2 and chip 4). Chips at the center are within adequate distance from the cold walls to be more impacted by the viscosity. The values representing isolines showed an augmentation as ε^* increased. The observation indicates that if temperature across the heated chips needs to be improved without impacting the flow stream, ε^* variation is an ideal selection to enhance the temperature gradient within the electronic equipment or unit.
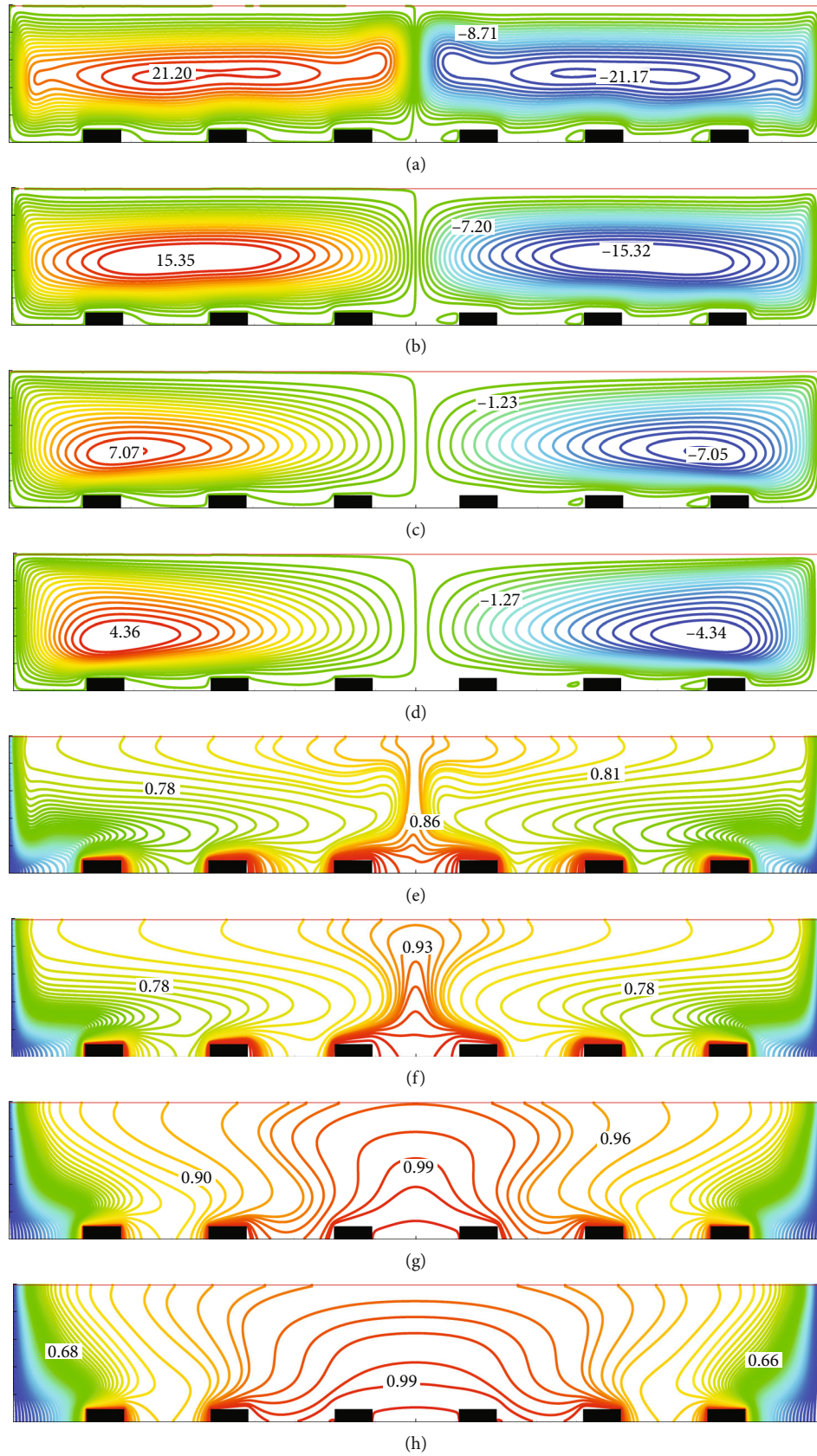
FIGURE 7: Streamlines and isotherms for (a, e) Ha = 0, (b, f) Ha = 20, (c, g) Ha = 60, and (d, h) Ha = 80 while Ra = 10^5, $\varepsilon^* = 3$, and $\phi = 0.04$.
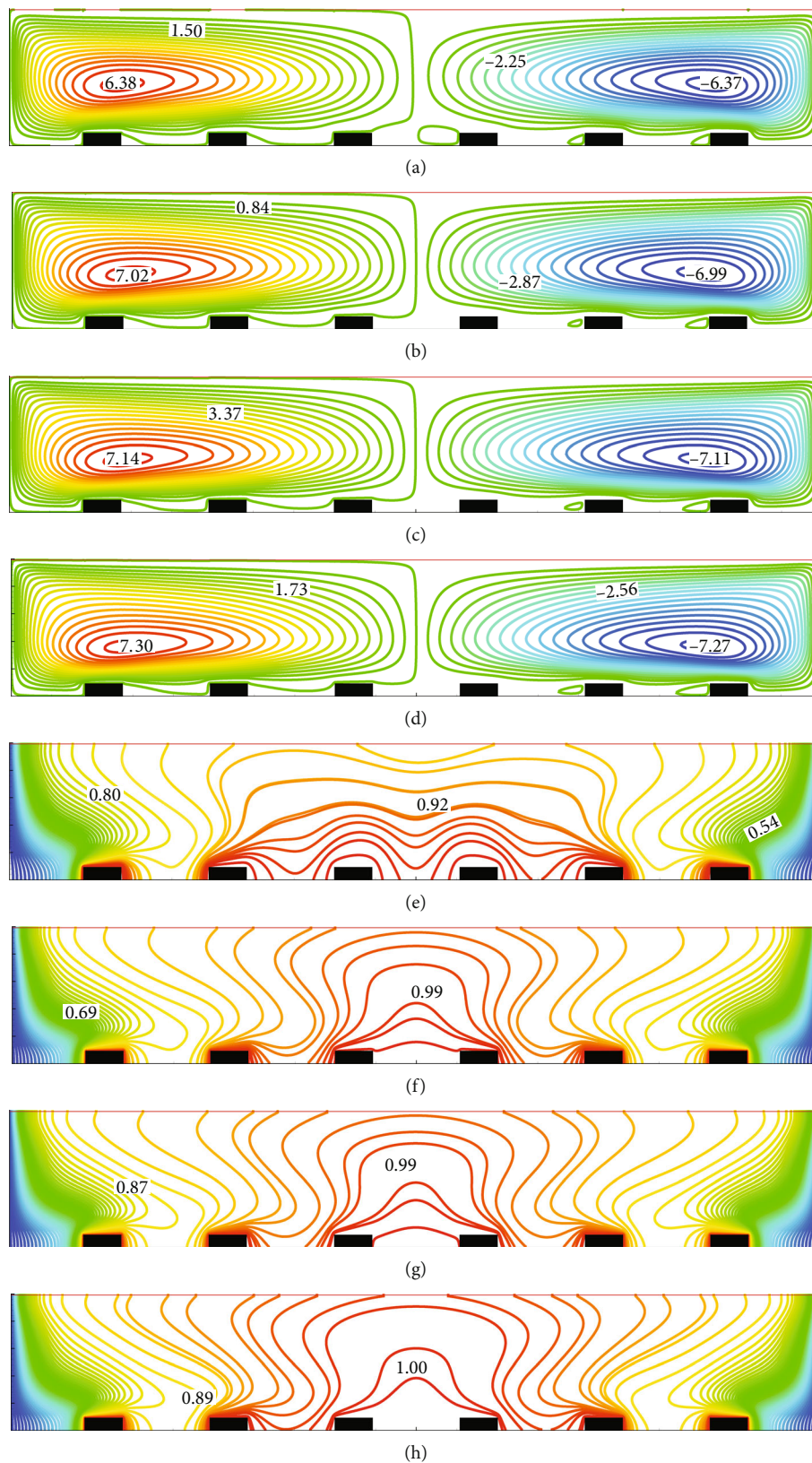
FIGURE 8: Contours of streamline and isotherm for viscosity variation parameter for (a, e) $\varepsilon^* = 0$, (b, f) $\varepsilon^* = 2$, (c, g) $\varepsilon^* = 3$, and (d, h) $\varepsilon^* = 5$ while Rayleigh number Ra = 10^5, Hartman number Ha = 60, and volume fraction $\phi = 0.04$.
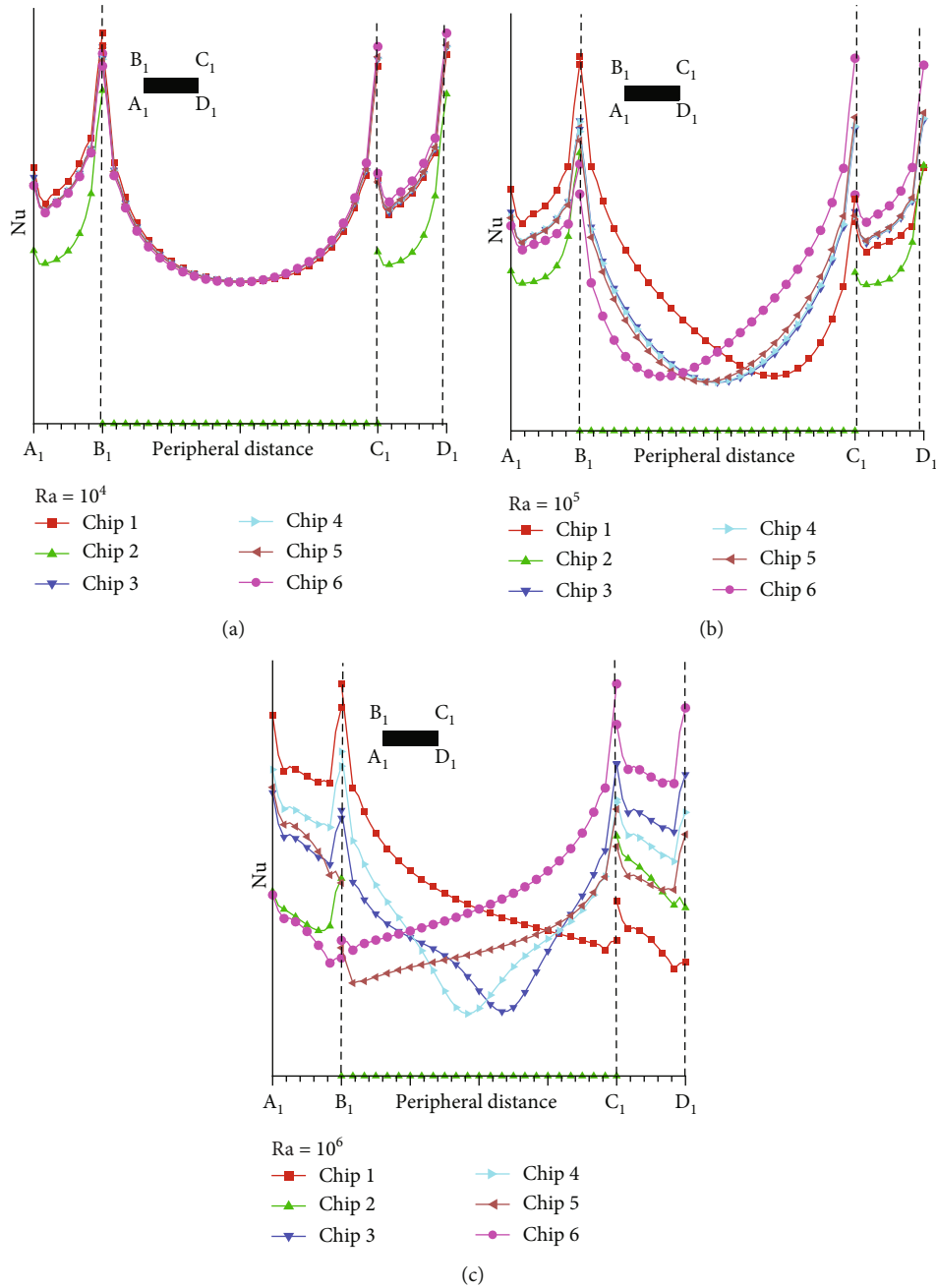
Figure 9: Local Nusselt number Nu analysis for the six chips case at (a) Ra = 10^4, (b) Ra = 10^5, and (c) Ra = 10^6 for hybrid case while ϕ = 0.04, Ha = 40, and ε^* = 2 are fixed.

6.4. Impact of Rayleigh Number on Local Nusselt Number.
The local Nu number is a dimensionless parameter used to describe the convective heat transfer rate in a fluid system. The performance of a hybrid nanofluid system is significantly influenced by the local Nu number, which can also serve as a helpful indicator for assessing the outcomes from the simulation. Numerous variables, including the fluid characteristics, the boundary conditions, and the presence of suspended nanoparticles, might affect the local Nu numbers. A hybrid nanofluid system's local Nusselt number can be affected by including nanoparticles by altering the fluid's thermal conductivity, viscosity, and flow patterns.

As the fluid transfers heat more effectively from one point to another, a rise in the local Nu number might signify increased heat transfer capability.

The current study has three cases that compare the simulation results: the hybrid nanofluid, alumina, and copper. This section will analyze it chronologically, considering the peripheral distance of local Nu variations. In plotting the local Nu number, the peripheral distance refers to the radial position or distance from a central axis. In this context, the local Nu number is plotted as a function of peripheral distance to visualize the spatial distribution of heat transfer within the system. The local Nu number at a given peripheral distance
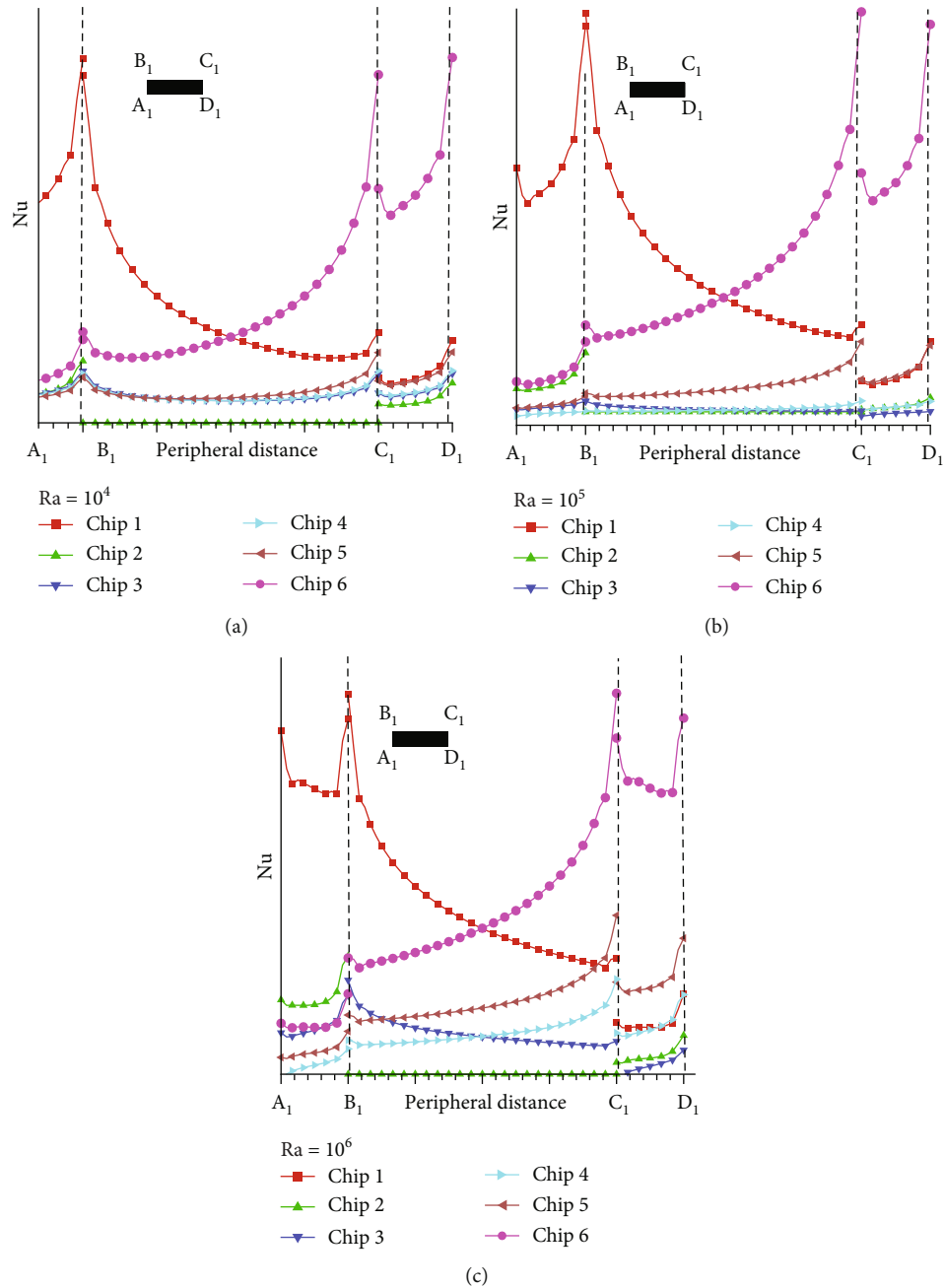
FIGURE 10: Local Nusselt number Nu analysis for the six chips case at (a) $Ra = 10^4$, (b) $Ra = 10^5$, and (c) $Ra = 10^6$ for alumina while $\phi = 0.04$, $Ha = 40$, and $\varepsilon^* = 2$ are fixed.

represents the heat transfer rate per unit area at that location. By plotting the local Nu number as a function of peripheral distance, it is possible to see how the heat transfer rate varies with position and identify any spatial variations or trends in the heat transfer behavior. The peripheral distance is an important variable when plotting the local Nu number because it provides information about the heat transfer location within the system. This can be useful for understanding and optimizing the system's thermal performance and comparing simulation results.

To estimate and analyze the influence of the local Nusselt number on the chips, the first variation of Ra numbers

has been taken for getting the simulation results where other parameters were kept constant such as $\phi = 0.04$, $Ha = 40$, and $\varepsilon^* = 2$ for Figure 9. The observation indicates the surface heat transfer rate for the hybrid case. The heated left side of the chip was represented by $A_1 B_1$, the chip's top side by $B_1 C_1$, and the chip's right side by $C_1 D_1$, allowing for a more in-depth look at how heat is transferred from the chip to the surroundings. Six chips have been considered for analyzing the heat transfer rate here in terms of the local Nu number. It was found that the first and last chips exhibited larger Nu values, indicating more heat transfer from these two chips. So, in this case, near the cold walls, a larger
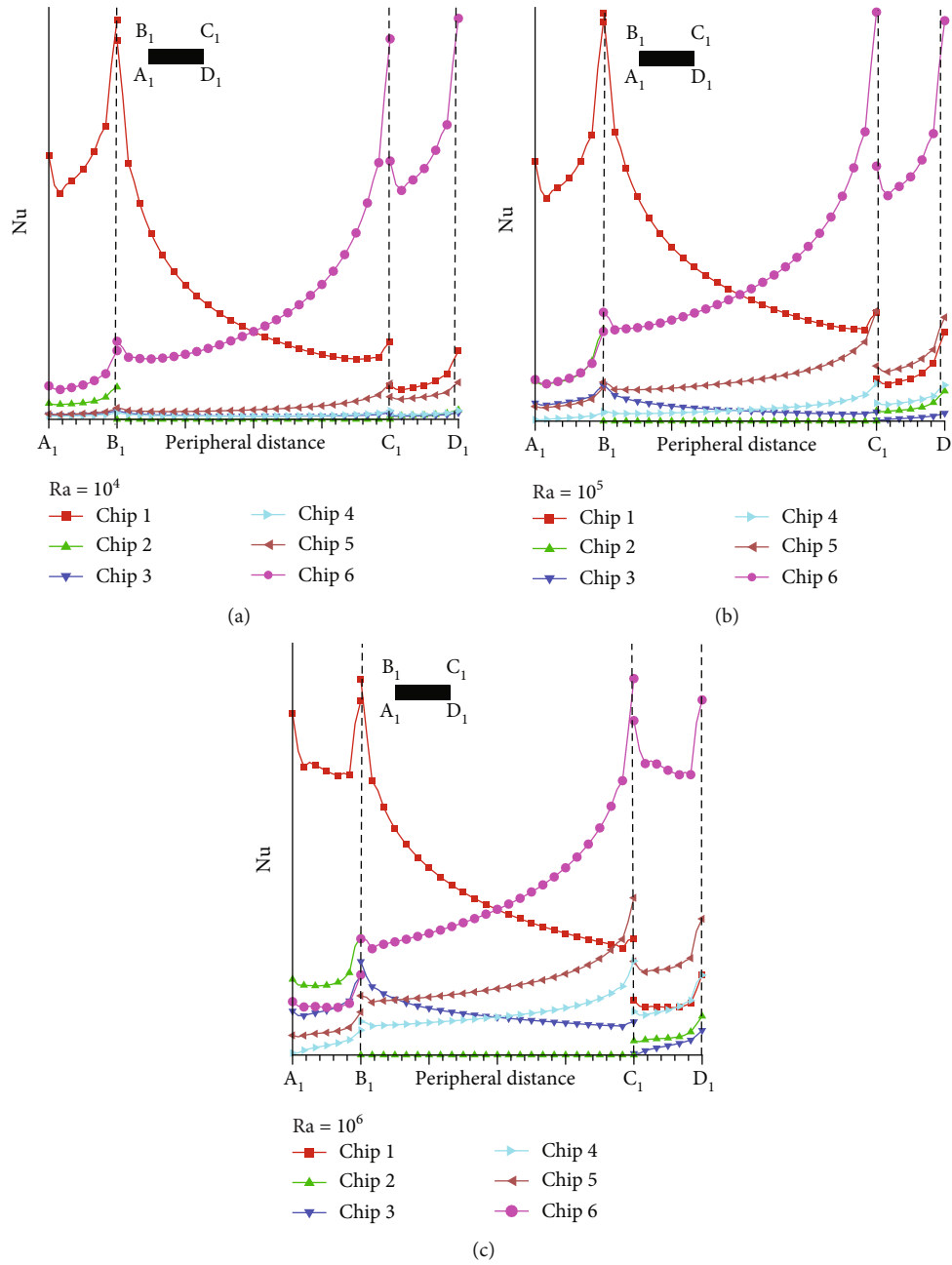
(a)

(b)

(c)

FIGURE 11: Local Nusselt number Nu analysis for the six chips case at (a) Ra = 10^4, (b) Ra = 10^5 and (c) Ra = 10^6 for copper while $\phi = 0.04$, Ha = 40, and $\varepsilon^* = 2$ are fixed.

temperature gradient was also found. From Figure 9(a), from a distance A_1-B_1 meaning the left side of chip 1 had the highest local Nu number, and from B_1-C_1 at this distance, chip 6 has the highest local Nu number, its gradient slowly increased from left side to right side and these two (chip one and chip six) gradients were higher than the rest of the chips. The observation was further clarified through Figure 9(b), where the greater peak values of chips 1 and 6 could be observed from A_1-B_1 and C_1-D_1, respectively, as Ra was increased from 10^4 to 10^5. The impact of buoyancy forces could be further cemented from Figure 9(c), where Ra = 10^6 was assigned. One thing could be noticed in chip

4, which showcased further dominance in peak values than chip 2 and chip 3. In this scenario, chip 4 seems to have improved local heat transfer. This observation could be further cross-checked with the findings from Figures 7(e)–7(h), where isolines across chip four were increasing in terms of density in the presence Ha number and ϕ. Therefore, the observation on the hybrid case in terms of local Nu number suggests that the temperature could be locally controlled across different chips by simply tuning the buoyancy force keeping Ha, ε^*, and ϕ constant and nonzero.

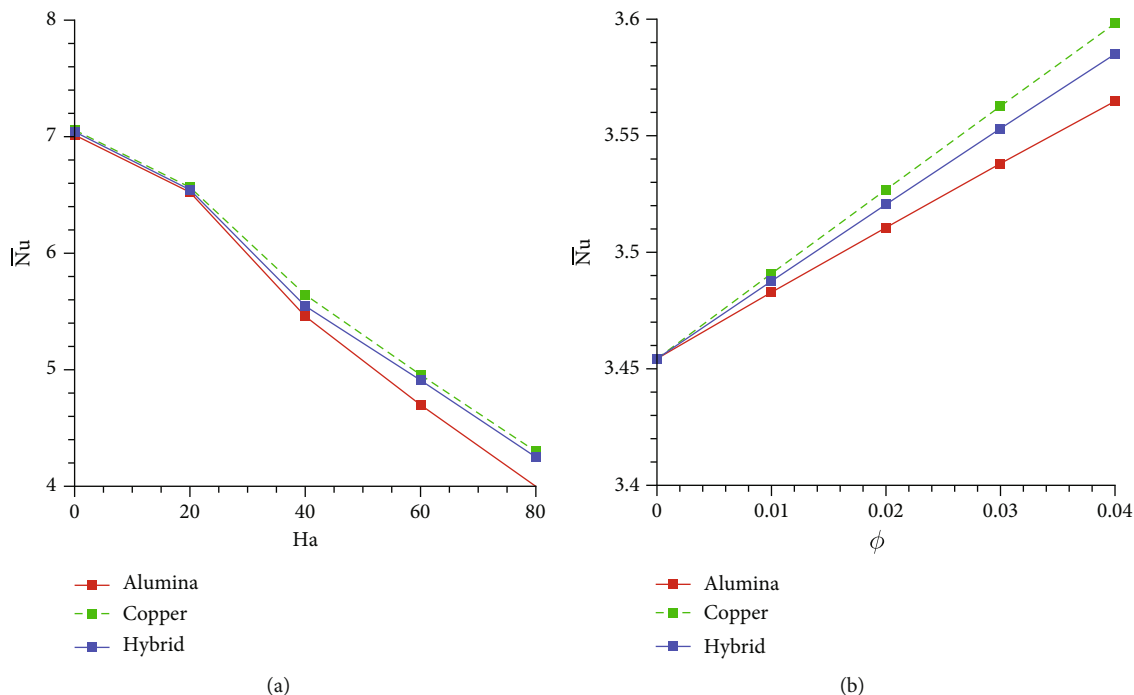Figure 10 depicts the variations in local Nu numbers as a function of Ra number only in the presence of alumina. It is

FIGURE 12: (a) Hartmann number variation where Ra = 10^5 and $\phi = 0.04$ are fixed and (b) volume fraction variation, where Ha = 20 and Ra = 10^5 are fixed to show average Nusselt number for Al, Cu, and hybrid case.

apparent from Figure 10 that the local Nu number distribution was less significant for only alumina than that of the hybrid case, as shown in Figure 9. However, chip one and chip 6 maintained the dominance as before. The rest of the chips exhibited substantially lower heat transmission rates locally. Chips 1 and 6 were the closest to the left and right cold walls, respectively. Therefore, seeing the corresponding heated chips showcasing better local heat transfer made more sense. However, most of the equipment with multiple blocks or chips will require the rest of the components to function efficiently concurrently to improve thermal efficiency. In this case, only alumina cannot be a solution to that. This observation can be further validated with only the Cu case in the following paragraph.

In the final part of this segment, the impact of only Cu could be observed on local Nu numbers, as shown in Figure 11. The overall observation suggested that as Ra increased, the local heat transfer was more noticeable across chips 1 and 6, like only the alumina case. This pattern confirmed the hypothesis and assumption discussed above, indicating that nonhybrid case may not be entirely suitable for locally controlled heat transmission across multiple heated chips despite increasing the Ra number to 10^6. However, the three cases mentioned above were only discussed in terms of variable Ra. It was necessary to observe the changes by varying Ha and ϕ as well. Instead of repeating the observation for local Nu, this investigation was conducted for $\bar{\text{Nu}}$ in the next section.

6.5. Effects on Average Nusselt Number

6.5.1. Variations in Hartmann Number and Volume Fraction of Nanoparticles. Figure 12(a) shows the variation of Hart-

mann number for alumina, copper, and hybrid case together by keeping Ra = 10^5 and $\phi = 0.04$ constant. It could be observed that Cu showed comparatively better $\bar{\text{Nu}}$ values, and alumina demonstrated the lowest among the cohort. Typically, as Ha increased, $\bar{\text{Nu}}$ decreased, which was expected as the influence of the magnetic field was discussed earlier in several places. However, the impact of Ha was only visible at Ha > 30. Although Cu led the parity, the difference was not mammoth compared to the hybrid. This could be explained by revisiting Table 1 where Cu had approximately 903% greater thermal conductivity than alumina. Therefore, $\bar{\text{Nu}}$ got reduced since it only states the mean values of heat transfer. Furthermore, the maximum $\bar{\text{Nu}}$ value does not necessarily mean the best solution for a specific application. The overall efficacy could be a significant concern regarding Cu, which was also observed in local Nu distribution, where most of the chips remained quite inactive compared to chips 1 and 6. Considering both local and average Nu, the hybrid option should still be a better selection. This could be further validated by varying ϕ in the process. Unless Cu varied significantly with increasing ϕ, the hybrid should remain the best alternative in improving the thermal efficiency of the electronic equipment.

The impact of ϕ on $\bar{\text{Nu}}$ is shown in Figure 12(b). Including ϕ effectively improved $\bar{\text{Nu}}$ values due to improved thermal conductivity, regardless of the rheology of the fluid. However, the marginal dominance of Cu could be observed here as well as ϕ increased. Each fraction of Cu increases the overall heat transfer due to more efficient thermal properties. However, considering the differences with hybrid cases across different ϕ, Cu alone did not bring massive improvement within the system. Considering the marginal improvement
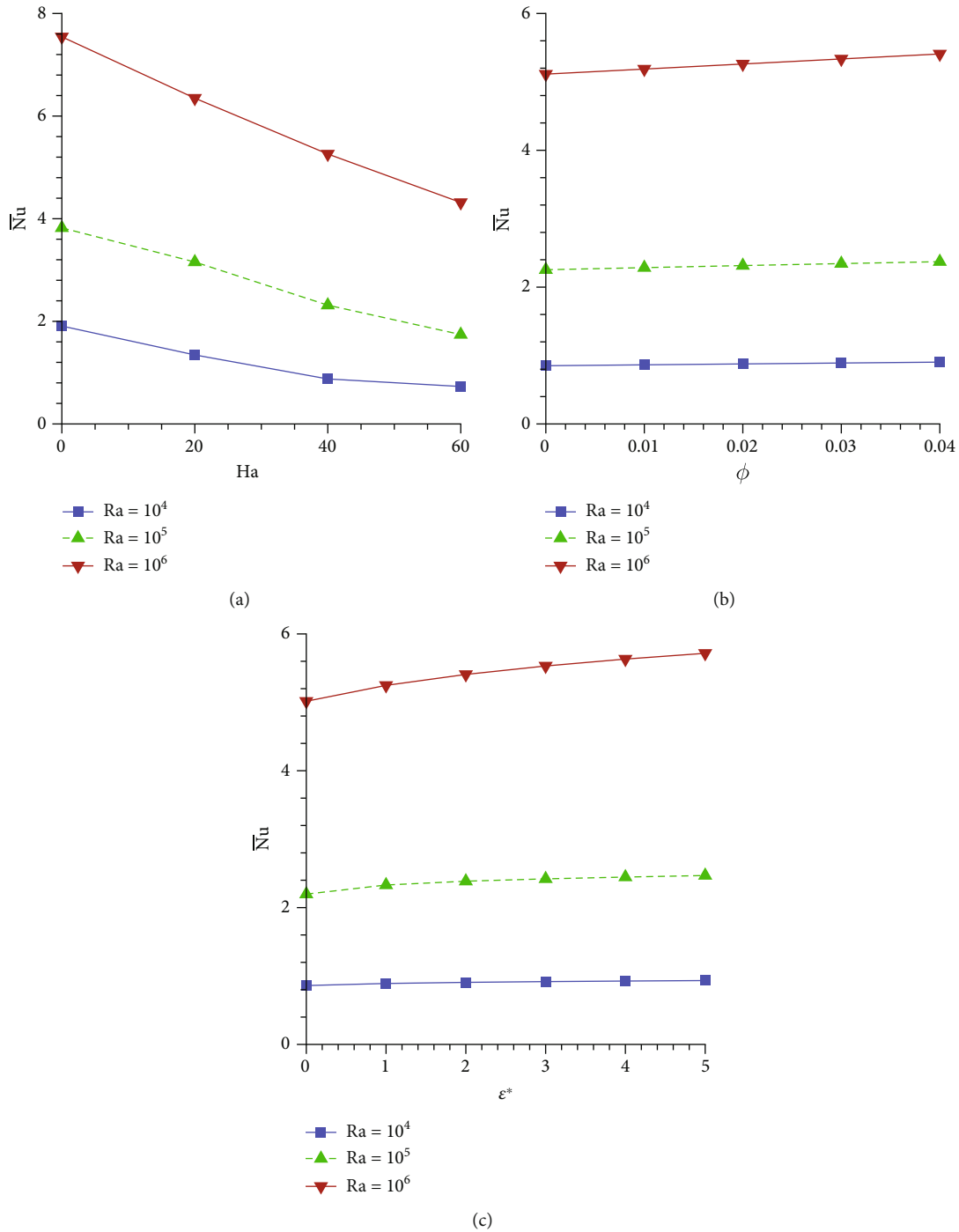
(a)

(b)

(c)

FIGURE 13: For different Rayleigh numbers, (a) variation of Hartmann number where $\varepsilon^* = 2$ and $\phi = 0.02$, (b) variation of volume fraction where Ha = 40 and $\varepsilon^* = 2$, and (c) variation of viscosity variation parameter where Ha = 40 and $\phi = 0.02$ are fixed to show average Nusselt number for hybrid case.

in local heat transfer earlier, Cu cannot be completely an efficient element for multiple heated chips. While it improves the average heat transfer rate, the improvement was less influential in local heat transfer. Overall, the hybrid option should have opted to control a cooling system or appropriate electronic equipment with multiple heated chips to have more control over the functional ability. Nevertheless, it will be

interesting to see if the results obtained here remain consistent for hybrid nanofluid at augmented Ra numbers, which were not discussed here.

6.5.2. Influence of Rayleigh Number on Hybrid Nanofluid. So far, hybrid nanofluid has been observed to be comparatively better overall. However, the sensitivity should also be tested

in terms of varying buoyancy within the system. This test was conducted at three different Ra numbers by varying Ha, ϕ, and ε^* in each segment below.

The impact of Ha numbers on $\bar{N}u$ on each Ra number could be seen in Figure 13(a). The observation matched the earlier discussion and has not been repeated here. However, the local maxima and minima of $\bar{N}u$ kept improving as Ra augmented. However, the difference almost doubled as Ra increased from 10^5 to 10^6. It is anticipated that the difference would have gotten greater if a further augmented Ra was imposed within the system. The impact of Ra = 10^6 was also seen in terms of varying ϕ as shown in Figure 13(b). While the improvement was insignificant at Ra = 10^4 and 10^5, the increased values of $\bar{N}u$ could be seen in terms of Ra = 10^6 despite imposing Ha = 40 within the system. The increasing rate will be greater at lower or no Ha number, but considering the MHD effect of the present study, this was not implemented. Therefore, Ha = 40 was used as a parameter here. Similar characteristics were observed in terms of increasing ε^* as temperature-dependent viscosity also adds a restriction to the fluid mobility as shown in Figure 13(c). Combining Figures 13(b) and 13(c), this was an indication that improving ϕ alone will not improve thermal efficiency. It is also important to augment Ra in such a way that the hybrid nanofluid can overcome the restrictions imposed due to the Ha number and ε^*.

6.5.3. Overall Observations and Data Extraction. The overall observations on $\bar{N}u$ have been depicted in Table 5, where the effects of Ra, ϕ, and Ha numbers on $\bar{N}u$ were tabulated for hybrid nanofluid at a fixed ε^*. The data suggested that increasing Ra and ϕ augmented $\bar{N}u$ values regardless of the values of Ha number within the system. However, the highest values of $\bar{N}u$ were recorded in the absence of Ha numbers as seen from the column stating "Ha = 0" in Table 5. Similar characteristics were also noticed in Table 6, where ε^* was varied keeping ϕ fixed.

For a higher average Nusselt number, the rectangular cavity wall can rapidly transport heat from the heaters to the cold walls. While varying the volume fraction, $\bar{N}u$ increases as Ra climbs from 10^4 to 10^6. This is evident from the table that Ra clearly describes the fluid velocity, with a smaller number implying laminar flow and then a larger value representing increasing heat transfer more quickly. As a result, an increase in Ra generates the buoyancy force to speed up, leading to increased flow circulation intensity because Ra is relevant to the proportion of buoyancy force toward the product of thermal viscosity and thermal diffusivity. As a result, the average Nusselt number for Ra = 10^6 is higher than for Ra = 10^4 and Ra = 10^5. Consequently, a greater buoyancy force helps in effective heat transfer than the flow attained for Ra = 10^6. While varying volume fraction $0.00 \leq \phi \leq 0.02$ for fixed Ra = 10^6, the average Nusselt number increases 1.3% where no magnetic field effect is considered. Again for varying volume fraction $0.02 \leq \phi \leq 0.04$, average Nusselt number increases with 1.12%. Again if Ha was considered and if Ha value increased from 0 to 20, ϕ = 0.00, and Ra = 10^6, average Nusselt number decreased

TABLE 5: Average Nusselt number (Nu_{avg}) for hybrid nanofluid when $\varepsilon^* = 2$.

Ra	ϕ	Average Nusselt number			
		Ha = 0	Ha = 20	Ha = 40	Ha = 60
	0.00	1.8779	1.3244	0.8511	0.6981
	0.01	1.8934	1.3348	0.8642	0.7142
Ra = 10^4	0.02	1.9083	1.3449	0.8771	0.7302
	0.03	1.9180	1.3548	0.8906	0.7471
	0.04	1.9319	1.3644	0.9039	0.7639
	0.00	3.7216	3.0702	2.2539	1.6962
	0.01	3.7716	3.1135	2.2849	1.7196
Ra = 10^5	0.02	3.8215	3.1559	2.3148	1.7422
	0.03	3.8707	3.1975	2.3438	1.7639
	0.04	3.9192	3.2382	2.3719	1.7849
	0.00	7.4462	6.4299	5.1131	4.1871
	0.01	7.4143	6.4676	5.1876	4.2517
Ra = 10^6	0.02	7.5448	6.4821	5.2616	4.3162
	0.03	7.5761	6.5077	5.3352	4.3803
	0.04	7.6304	6.5592	5.4081	4.4437

TABLE 6: Average Nusselt numbers for Ra and ε^* variation at a fixed $\phi = 0.04$.

Ra	ε^*	Average Nusselt number			
		Ha = 0	Ha = 20	Ha = 40	Ha = 60
	0	1.5437	1.1649	0.8606	0.7537
	1	1.7654	1.2715	0.8905	0.7634
Ra = 10^4	2	1.9318	1.3364	0.9073	0.7677
	3	2.0650	1.3817	0.9184	0.7711
	4	2.1741	1.4157	0.9266	0.7733
	5	2.2652	1.4426	0.9330	0.7752
	0	3.3891	2.9031	2.1967	1.6956
	1	3.7151	3.1148	2.3303	1.7559
Ra = 10^5	2	3.9192	3.2384	2.3859	1.7862
	3	4.0716	3.3289	2.4204	1.8058
	4	4.1953	3.3977	2.4462	1.8197
	5	4.3001	3.4566	2.4690	1.8305
	0	5.8888	5.9155	5.0162	4.2258
	1	7.2351	6.3661	5.2482	4.3588
Ra = 10^6	2	7.6722	6.6094	5.4082	4.4439
	3	7.7848	6.8581	5.5318	4.5069
	4	8.0890	6.9502	5.6329	4.5573
	5	8.3333	6.4496	5.7173	4.5987

with 13.65%. For the same case, if the volume fraction was increased to $\phi = 0.04$ and Ha = $0 \leq \phi \leq$ Ha = 20, the average Nusselt number decreased 14%. The decrement rate of heat transfer grew for developing fluids volume fraction and Hartmann number.

Another case has been considered for seeing the trends of the $\bar{N}u$ number. According to Table 6, the changes of
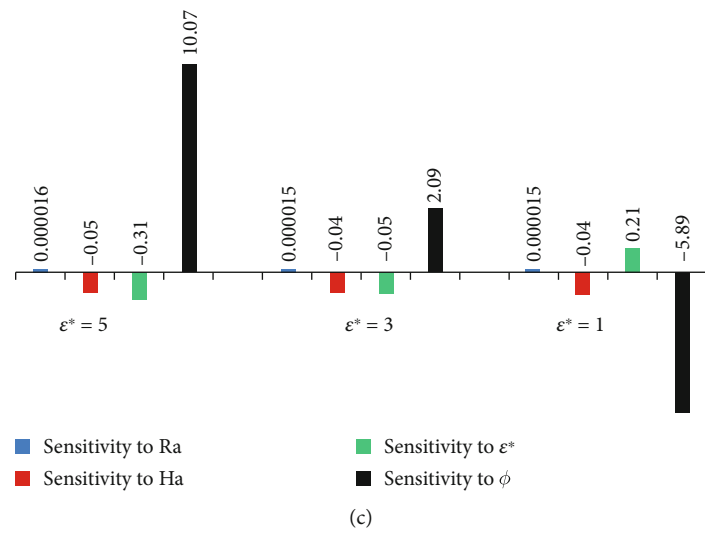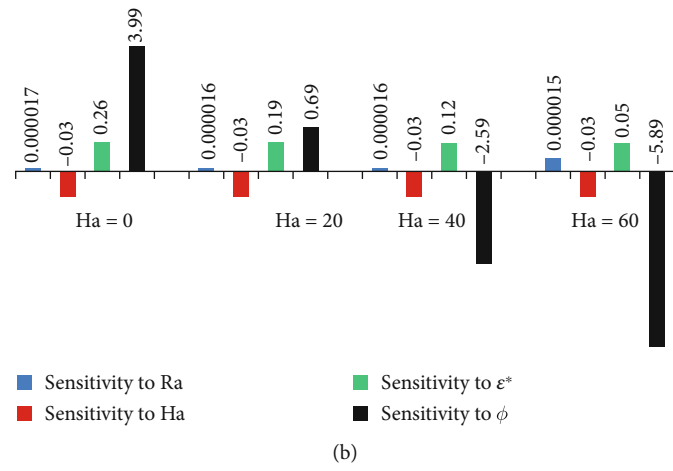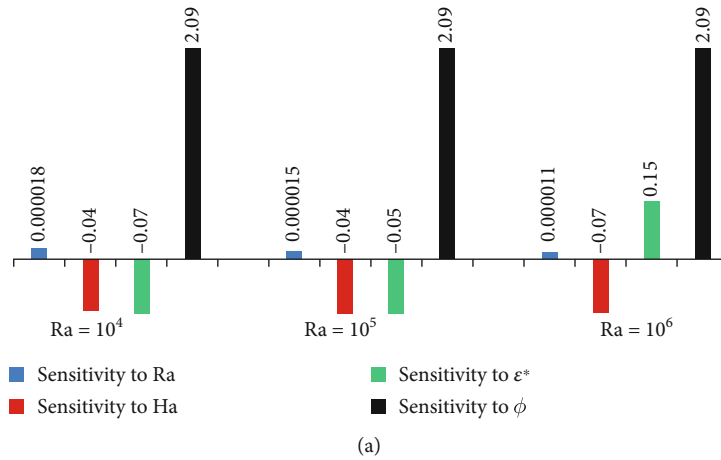
(a)

(b)

(c)

FIGURE 14: Continued.
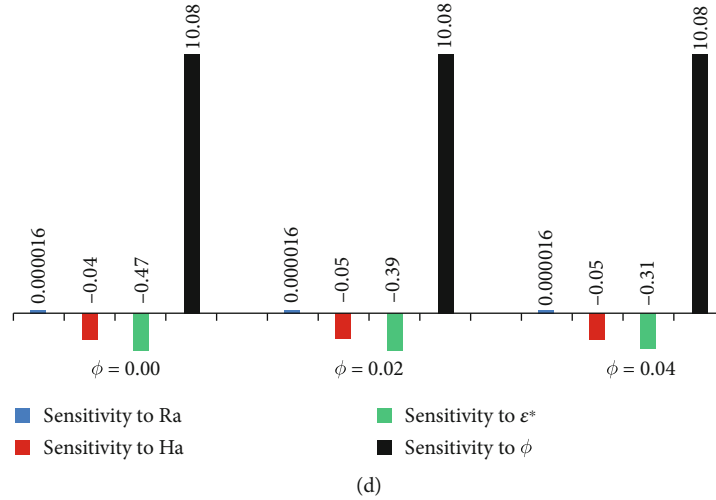
FIGURE 14: Sensitivity analysis for (a) $Ra = 10^4$, 10^5, and 10^6 for fixed $\varepsilon^* = 3$, $Ha = 60$, and $\phi = 0.04$; (b) $Ha = 0$, 20, 40, and 60 while $\varepsilon^* = 1$, $Ra = 10^5$, and $\phi = 0.0$; (c) $\varepsilon^* = 1$, 3, and 5 while $Ha = 60$, $Ra = 10^5$, and $\phi = 0.04$; and (d) $\phi = 0.00$, 0.02, and 0.04 for fixed $Ra = 10^5$, $Ha = 60$, and $\varepsilon^* = 5$.

the $\bar{N}u$ were visible, and maximum $\bar{N}u$ was obtained for the lowest value of the Hartmann number, and the opposite relation was found for the highest Hartmann number. For volume fraction $0.01 \leq \phi \leq 0.03$ and at fixed $Ha = 0$, the average Nusselt number increases with the percentage of 5.91. However, at the same range $0.01 \leq \phi \leq 0.03$ and at $Ha = 80$, this rising rate changed into 1.92. Increasing the volume fraction helped to grow the average Nusselt number. Still, the Hartmann number controlled this rate of increasing $\bar{N}u$ slowly, and it lowered the value of $\bar{N}u$, which was in line with the decreasing heat transfer and flow phenomena of the selected nanofluid for this project.

To summarise, it could be seen that increasing Ra, ϕ, and ε^* improved the heat transfer rate, while increasing Ha downgraded the heat transfer. While the simulated data always contained one or two static variables, analyzing the correlations within the input parameters concurrently was still significant to conclude the finding. Therefore, further statistical analyses have been conducted to develop more confidence in the findings of this study.

7. Sensitivity Analysis

Sensitivity analysis is employed to comprehend how modifications to one or more input variables or assumptions affect a model's or system's output. This can assist in locating potential model flaws. Sensitivity analysis is a basic method for determining a model's reliability; recognizing influential variables, uncertainty of input variables, and calculations; and assisting in making decisions [51, 52]. When input affects output, evaluation of uncertainty can be measured through sensitivity analysis [53]. Using the statistical regression model, the parametric correlations have been obtained for the average Nusselt number. The regression equation has been obtained by the Design-Expert software. Based on our obtained real data, the software suggested the correlation equation (32). The correlation equation using all parameters used in this study is as follows:

$$
\begin{aligned}
\bar{N}u =\ & 1.3088 + 0.00002Ra - 0.0232Ha + 0.3647\varepsilon^* \\
& - 2.86 \times 10^{-8}RaHa + 2.28 \times 10^{-7}Ra\varepsilon^* \\
& - 0.0034Ha\varepsilon^* - 0.1647Ha\phi + 3.9916\varepsilon^*\phi \\
& - 1.49 \times 10^{-11}Ra^2 - 0.0658\varepsilon^{*2}.
\end{aligned}
\tag{32}
$$

The elements that most significantly affected the response variability can be identified by looking at the correlation equation's coefficients. For the sensitivity test, we have taken the first derivative of the correlation (32) in terms of each parameter we have:

$$
\begin{aligned}
\frac{\partial \bar{N}u}{\partial Ra} =\ & 0.00002 - 2.86 \times 10^{-8}Ha + 2.28 \times 10^{-7}\varepsilon^* \\
& - 2.98 \times 10^{-11}Ra,
\end{aligned}
\tag{33}
$$

$$
\frac{\partial \bar{N}u}{\partial Ha} = -0.0232 - 2.86 \times 10^{-8}Ra - 0.0034\varepsilon^* - 0.1647\phi,
\tag{34}
$$

$$
\begin{aligned}
\frac{\partial \bar{N}u}{\partial \varepsilon^*} =\ & 0.3647 + 2.28 \times 10^{-7}Ra - 0.0034Ha \\
& + 3.9916\phi - 0.1316\varepsilon^*,
\end{aligned}
\tag{35}
$$

$$
\frac{\partial \bar{N}u}{\partial \varepsilon^*} = -0.1647Ha + 3.9916\varepsilon^*.
\tag{36}
$$

Here, sensitivity toward Ra, Ha, ε^*, and ϕ was calculated using Equations (33)–(36), respectively. Figure 14 shows the sensitivity test for all parameters. The bar graph shows that sensitivity for ϕ is at its highest point. Changing a minimal volume fraction will have the highest impact on this model. This model can be controlled in a better way through this parameter (ϕ). This input variable will have the highest effect on the model's output. In this case, increasing the volume

fraction will increase the average Nusselt number. It will then increase the fluid flow and heat transfer rate faster, with a positive sensitivity magnitude. In Figure 14(a), Ra variation was considered. It is shown that Ra has a positive sensitivity, while Ha shows a negative sensitivity throughout in all cases. As increasing Ha has the damping effect on fluid flow, as a result, fluid velocity retards, which is already discussed in Section 6.2. Among all the parameters, ε^* shows both characteristics and shows both positive and negative sensitivity depending on the scenario.

8. Conclusion

The 2D multiple-relaxation-time lattice Boltzmann approach coupled with GPU computing was used in this paper to thoroughly examine the effect of MHD on the convection of Newtonian hybrid nanofluid by considering six heated chips. The study is extremely important for thermal and fluid dynamics research. This advanced modeling method enables a thorough and precise examination of the complicated interactions between natural convection, magnetic fields, and complex heat transfer properties of the hybrid nanofluids. The study investigates the influence of several dimensionless characteristics such as the Rayleigh number $(10^4 \leq \text{Ra} \leq 10^6)$, volume fraction $(0.00 \leq \phi \leq 0.04)$, Hartmann number $(0 \leq \text{Ha} \leq 60)$, and viscosity variation parameter $(0 \leq \varepsilon^* \leq 5)$ in terms of streamlines, isotherms, and peripheral local and average Nusselt numbers for the heated chips. Furthermore, the sensitivity test has been done using response surface methodology to statistically investigate the influence and correlations among the parameters on $\bar{\text{Nu}}$. The findings from this study could be summarised as the following:

(i) Copper is marginally better in producing $\bar{\text{Nu}}$ than hybrid nanofluid. However, local Nu distribution was overall better for hybrid nanofluid across all heated chips. Electronic equipment with multiple heated blocks will have a much more efficient local temperature-controlling mechanism across each chip if a hybrid nanofluid is used over copper or alumina. In addition, the distance between each heated chip should have thermal insulation to improve the equipment's durability and heat transferability

(ii) Introducing a magnetic field can lessen the convective heat transfer and fluid movement in the rectangular enclosure. $\bar{\text{Nu}}$ decreased as Ha number increased due to dominance of imposed Lorentz force. If overheating or excessive heat generation remains an issue within a device, imposing a magnetic field through tuning Ha number is a great alternative. $\bar{\text{Nu}}$ was obtained to be maximum in the absence of Ha number

(iii) Increasing buoyancy force within the system significantly augmented $\bar{\text{Nu}}$

(iv) Inclusion of ϕ and ε^* is a good alternative to control the thermal efficiency of a unit with multiple heated chips

(v) The present research's robustness has been analyzed through sensitivity analysis

(vi) For increased Ha from 0 to 20, while $\phi = 0.0$ and Ra $= 10^6$, average Nusselt number decreased with 13.65%. For the same case, if the volume fraction was increased to $\phi = 0.04$, then the average Nusselt number decreased 14%

(vii) While varying volume fraction $0.00 \leq \phi \leq 0.02$ for fixed Ra $= 10^6$, the average Nusselt number increases 1.3% where no magnetic field effect is considered

(viii) It is shown that Ra has a positive sensitivity, while Ha shows a negative sensitivity throughout in all cases, and ϕ has the highest sensitivity to the overall system

(ix) The present problem can be extended for the various non-Newtonian model. Using more advance numerical model, the present work can be upgraded with more robust results

(x) The knowledge of the present problem can be used in more advance and practical applications of hybrid nanofluid with magnetic field effect for controlling heat transfer rate

Nomenclature

B_0: Magnetic force (kg s^{-2} A^{-1})
C_p: Specific heat (J kg^{-1} K^{-1})
f: Probability distribution function for the velocity field
g_o: Gravitational acceleration (ms^{-2})
g: Probability distribution function for the temperature field
Ha: Hartmann number
k: Thermal conductivity (J m^{-1} s^{-1} K^{-1})
m: Vector moments
M: Collision matrix for the velocity field
N: Collision matrix for the temperature field
$\bar{\text{Nu}}$: Nusselt number (average)
Pr: Prandtl number
Ra: Rayleigh number
T: Temperature (K)
T_o: Bulk temperature (K)
$\breve{u}, \breve{v}$: Dimensional mid-x and mid-y velocity components (ms^{-1})
u, v: Dimensionless mid-x and mid-y velocity components
$\bar{x}, \bar{y}$: Dimensional coordinates (m)
x, y: Dimensionless coordinates.

Greek Letters

ε^*: Viscosity variation parameter
α: Thermal diffusivity (m^2 s^{-1})
β: Thermal expansion coefficient (K^{-1})
μ: Dynamic viscosity (kg m^{-1} s^{-1})
ν: Kinematic viscosity (m^2 s^{-1})
ρ: Fluid density (kg m^{-3})

σ: Electrical conductivity (S/m)
ϕ: Volume fraction
ψ: Dimensionless stream function.

Data Availability

No third-party data was used here.

Conflicts of Interest

There are no conflicts of interest.

Acknowledgments

References

[1] H. Qu, Y. Yang, Y. Chang et al., "On-chip integrated multiple microelectromechanical resonators to enable the local heating, mixing and viscosity sensing for chemical reactions in a droplet," *Sensors and Actuators B: Chemical*, vol. 248, pp. 280–287, 2017.

[2] P. Wan, L. Gao, and J. Wang, "Approaching ultra-low thermal conductivity in β-sic nanoparticle packed beds through multiple heat blocking mechanisms," *Scripta Materialia*, vol. 128, pp. 1–5, 2017.

[3] H. Shahid, I. Yaqoob, W. A. Khan, and A. Rafique, "Mixed convection in an isosceles right triangular lid driven cavity using multi relaxation time lattice Boltzmann method," *International Communications in Heat and Mass Transfer*, vol. 128, article 105552, 2021.

[4] J. Baliti, Y. Elguennouni, M. Hssikou, and M. Alaoui, "Simulation of natural convection by multirelaxation time lattice Boltzmann method in a triangular enclosure," *Fluids*, vol. 7, no. 2, p. 74, 2022.

[5] A. Boutra, A. Bourada, and Y. Benkahla, "Free convection of Ostwald-de Waele fluid within square enclosure equipped with heat-generating circular solid: MRT-LBM simulation," *Journal of the Taiwan Institute of Chemical Engineers*, vol. 149, article 104999, 2023.

[6] S. R. Bhopalam and D. A. Perumal, "Numerical analysis of fluid flows in L-shaped cavities using lattice Boltzmann method," *Applications in Engineering Science*, vol. 3, article 100016, 2020.

[7] M. J. Anee, S. Siddiqa, M. F. Hasan, and M. M. Molla, "Lattice Boltzmann simulation of natural convection of ethylene glycol-alumina nanofluid in a C-shaped enclosure with MFD viscosity through a parallel computing platform and quantita-

tive parametric assessment," *Physica Scripta*, vol. 98, no. 9, article 095203, 2023.

[8] A. Fattahi, N. Hajialigol, M. Delpisheh, and N. Karimi, "Lattice-Boltzmann numerical simulation of double-diffusive natural convection and entropy generation in an n-shaped partially heated storage tank," *Engineering Analysis with Boundary Elements*, vol. 146, pp. 105–118, 2023.

[9] H. Younes, M. Mao, S. S. Murshed, D. Lou, H. Hong, and G. Peterson, "Nanofluids: key parameters to enhance thermal conductivity and its applications," *Applied Thermal Engineering*, vol. 207, article 118202, 2022.

[10] R. Lenin, P. A. Joy, and C. Bera, "A review of the recent progress on thermal conductivity of nanofluid," *Journal of Molecular Liquids*, vol. 338, article 116929, 2021.

[11] A. Dezfulizadeh, A. Aghaei, A. H. Joshaghani, and M. M. Najafizadeh, "An experimental study on dynamic viscosity and thermal conductivity of water- Cu-SiO_2-MWCNT ternary hybrid nanofluid and the development of practical correlations," *Powder Technology*, vol. 389, pp. 215–234, 2021.

[12] D. Chatterjee, N. Biswas, N. K. Manna, and S. Sarkar, "Effect of discrete heating-cooling on magneto-thermal-hybrid nanofluidic convection in cylindrical system," *International Journal of Mechanical Sciences*, vol. 238, article 107852, 2023.

[13] K. D. Goswami, A. Chattopadhyay, and S. K. Pandit, "Magneto-thermogravitational convection for hybrid nanofluid in a novel shaped enclosure," *International Journal of Mechanical Sciences*, vol. 234, article 107674, 2022.

[14] A. Siricharoenpanich, S. Wiriyasart, A. Srichat, and P. Naphon, "Thermal cooling system with Ag/Fe_3O_4 nanofluids mixture as coolant for electronic devices cooling," *Case Studies in Thermal Engineering*, vol. 20, article 100641, 2020.

[15] Z. Tang, C. Qi, Z. Tian, and L. Chen, "Thermal management of electronic components based on new wave bio-inspired structures and nanofluids," *International Communications in Heat and Mass Transfer*, vol. 131, article 105840, 2022.

[16] A. Moita, A. Moreira, and J. Pereira, "Nanofluids for the next generation thermal management of electronics: a review," *Symmetry*, vol. 13, no. 8, p. 1362, 2021.

[17] M. Nemati, M. Sefid, A. Karimipour, and A. J. Chamkha, "Computational thermal performance analysis by LBM for cooling a hot oval object via magnetohydrodynamics non-Newtonian free convection by using magneto-ferrofluid," *Journal of Magnetism and Magnetic Materials*, vol. 577, article 170797, 2023.

[18] J. A. Eastman, S. Choi, S. Li, W. Yu, and L. Thompson, "Anomalously increased effective thermal conductivities of ethylene glycol-based nanofluids containing copper nanoparticles," *Applied Physics Letters*, vol. 78, no. 6, pp. 718–720, 2001.

[19] T. Vijaybabu and K. B. NB, "Significance of porous elliptical cylinder on the MHD natural convection," *International Journal of Mechanical Sciences*, vol. 237, article 107792, 2023.

[20] M. Nemati and M. Sefid, "The possibility of availing active and passive methods to achieve a flow with desirable characteristics via using the lattice Boltzmann method," *Engineering Analysis with Boundary Elements*, vol. 146, pp. 786–807, 2023.

[21] Z. Li, M. Sheikholeslami, A. S. Mittal, A. Shafee, and R.-u. Haq, "Unsteady magneto-hydrodynamics flow between two orthogonal moving porous plates," *The European Physical Journal Plus*, vol. 134, no. 1, pp. 1–10, 2019.

[22] A. Hossain, P. Nag, and M. M. Molla, "Mesoscopic simulation of MHD mixed convection of non-Newtonian ferrofluids with

a non-uniformly heated plate in an enclosure," *Physica Scripta*, vol. 98, no. 1, article 015008, 2022.

[23] S. N. Nia, F. Rabiei, M. Rashidi, and T. Kwang, "Lattice Boltzmann simulation of natural convection heat transfer of a nanofluid in a L-shape enclosure with a baffle," *Results in Physics*, vol. 19, article 103413, 2020.

[24] M. Sheikholeslami, H. Keramati, A. Shafee, Z. Li, O. A. Alawad, and I. Tlili, "Nanofluid MHD forced convection heat transfer around the elliptic obstacle inside a permeable lid drive 3D enclosure considering lattice Boltzmann method," *Physica A: Statistical Mechanics and its Applications*, vol. 523, pp. 87–104, 2019.

[25] M. Islam, M. F. Hasan, S. Bhowmick, M. Kamrujjaman, and M. M. Molla, "GPU-optimized LBM-MRT simulation of free convection and entropy generation of non-Newtonian power-law nanofluids in a porous enclosure at REV scale," *International Journal of Ambient Energy*, vol. 44, no. 1, pp. 995–1016, 2023.

[26] L. Wang, X. Yang, C. Huang, Z. Chai, and B. Shi, "Hybrid lattice Boltzmann-TVD simulation of natural convection of nanofluids in a partially heated square cavity using Buongiorno's model," *Applied Thermal Engineering*, vol. 146, pp. 318–327, 2019.

[27] B. Magacho, H. S. Tavares, L. Moriconi, and J. Loureiro, "Double multiple-relaxation-time model of lattice-Boltzmann magnetohydrodynamics at low magnetic Reynolds numbers," *Physics of Fluids*, vol. 35, no. 1, 2023.

[28] M. Nemati and A. J. Chamkha, "Examination of effective strategies on changing the amount of heat transfer and entropy during non-Newtonian magneto-nanofluid mixed convection inside a semi-ellipsoidal cavity," *Journal of Magnetism and Magnetic Materials*, vol. 578, article 170652, 2023.

[29] T. Zhang and D. Che, "Double MRT thermal lattice Boltzmann simulation for MHD natural convection of nanofluids in an inclined cavity with four square heat sources," *International Journal of Heat and Mass Transfer*, vol. 94, pp. 87–100, 2016.

[30] P. Karki and K. Gangawane, "Study of magnetohydrodynamics-based-mixed convection & entropy generation within the rectangular enclosure with two obstacles for Cu-SiO$_2$ multiwalled carbon nanotubes ternary hybrid nanofluids," *Numerical Heat Transfer, Part A: Applications*, pp. 1–23, 2023.

[31] S. Das, S. Sarkar, and R. Jana, "Feature of entropy generation in Cu-Al$_2$O$_3$/ethylene glycol hybrid nanofluid flow through a rotating channel," *Bionanoscience*, vol. 10, no. 4, pp. 950–967, 2020.

[32] M. Sheikholeslami, M. Rashidi, T. Hayat, and D. Ganji, "Free convection of magnetic nanofluid considering MFD viscosity effect," *Journal of Molecular Liquids*, vol. 218, pp. 393–399, 2016.

[33] M. Islam, S. A. Hai, P. Nag, and M. M. Molla, "Multiple-relaxation-time lattice Boltzmann simulation of free convection and irreversibility of nanofluid with variable thermophysical properties," *Physica Scripta*, vol. 96, no. 12, article 125031, 2021.

[34] F. Achard and J. C. Maxwell, "A treatise on electricity and magnetism, (1873)," in *Landmark Writings in Western Mathematics 1640-1940*, pp. 564–587, Elsevier, 2005.

[35] H. C. Brinkman, "The viscosity of concentrated suspensions and solutions," *The Journal of Chemical Physics*, vol. 20, no. 4, pp. 571–571, 1952.

[36] T. Mahalakshmi, N. Nithyadevi, H. F. Oztop, and N. Abu-Hamdeh, "Natural convective heat transfer of Ag-water nanofluid flow inside enclosure with center heater and bottom heat source," *Chinese Journal of Physics*, vol. 56, no. 4, pp. 1497–1507, 2018.

[37] J. Ling and A. Dybbs, "Forced Convection over a Flat Plate Submersed in a Porous Medium: Variable Viscosity Case," Tech. Rep., American Society of Mechanical Engineers, New York, NY, 1987.

[38] B. Trouette, "Lattice Boltzmann simulations of a time-dependent natural convection problem," *Computers & Mathematics with Applications*, vol. 66, no. 8, pp. 1360–1371, 2013.

[39] A. Rahman, P. Nag, and M. M. Molla, "Non-Newtonian effects on MHD thermosolutal free convection and entropy production of nanofluids in a rectangular enclosure using the GPU-based mesoscopic simulation," *Waves in Random and Complex Media*, pp. 1–33, 2022.

[40] Q. Liu, Y. L. He, Q. Li, and W. Q. Tao, "A multiple-relaxation-time lattice Boltzmann model for convection heat transfer in porous media," *International Journal of Heat and Mass Transfer*, vol. 73, pp. 761–775, 2014.

[41] M. M. Molla, M. J. Haque, M. A. I. Khan, and S. C. Saha, "GPU accelerated multiple-relaxation-time lattice Boltzmann simulation of convective flows in a porous media," *Frontiers in Mechanical Engineering*, vol. 4, p. 15, 2018.

[42] E. Ezzatneshan, A. Salehi, and H. Vaseghnia, "Study on forcing schemes in the thermal lattice Boltzmann method for simulation of natural convection flow problems," *Heat Transfer*, vol. 50, no. 8, pp. 7604–7631, 2021.

[43] J. Wang, D. Wang, P. Lallemand, and L.-S. Luo, "Lattice Boltzmann simulations of thermal convective flows in two dimensions," *Computers & Mathematcs with Applications*, vol. 65, no. 2, pp. 262–286, 2013.

[44] A. Mezrhab, M. A. Moussaoui, M. Jami, H. Naji, and M. Bouzidi, "Double MRT thermal lattice Boltzmann method for simulating convective flows," *Physics Letters A*, vol. 374, no. 34, pp. 3499–3507, 2010.

[45] G. Nardini, M. Paroncini, and R. Vitali, "Experimental and numerical analysis of the effect of the position of a bottom wall hot source on natural convection," *Applied Thermal Engineering*, vol. 92, pp. 236–245, 2016.

[46] N. Rudraiah, R. Barron, M. Venkatachalappa, and C. Subbaraya, "Effect of a magnetic field on free convection in a rectangular enclosure," *International Journal of Engineering Science*, vol. 33, no. 8, pp. 1075–1084, 1995.

[47] C. Ho, W. Liu, Y. Chang, and C. Lin, "Natural convection heat transfer of alumina-water nanofluid in vertical square enclosures: an experimental study," *International Journal of Thermal Sciences*, vol. 49, no. 8, pp. 1345–1353, 2010.

[48] P. Cardin and P. Olson, "Experiments on core dynamics," in *Treatise on Geophysics (Second Edition)*, G. Schubert, Ed., pp. 317–339, Elsevier, Oxford, 2nd edition, 2015.

[49] J. Hartmann and F. Lazarus, *Experimental Investigations on the Flow of Mercury in a Homogeneous Magnetic Field*, Munksgaard, 1937.

[50] R. J. Moreau, *Magnetohydrodynamics, vol. 3*, Springer Science & Business Media, 1990.

[51] F. Campolongo and R. Braddock, "The use of graph theory in the sensitivity analysis of the model output: a second order screening method," *Reliability Engineering & System Safety*, vol. 64, no. 1, pp. 1–12, 1999.

[52] A. Hossain, M. M. Molla, M. Kamrujjaman, M. Mohebujjaman, and S. C. Saha, "MHD mixed convection of non-Newtonian Bingham nanofluid in a wavy enclosure with temperature-dependent thermophysical properties: a sensitivity analysis by response surface methodology," *Energies*, vol. 16, no. 11, p. 4408, 2023.

[53] A. Saltelli, M. Ratto, T. Andres et al., *Global Sensitivity Analysis: The Primer*, John Wiley & Sons, 2008.